Hochschule für Angewandte Wissenschaften Hamburg
Hamburg University of Applied Sciences

Masterarbeit

Milan Koch

Transient Acoustic Simulation with Auralization

Technik und Informatik
Department Fahrzeugtechnik und Flugzeugbau

Faculty of Engineering and Computer Science
Department of Automotive and Aeronautical Engineering

Milan Koch

Transient Acoustic Simulation with Auralization

Masterarbeit eingereicht im Rahmen der Masterprüfung

im Studiengang Fahrzeugbau
am Department Fahrzeugtechnik und Flugzeugbau
der Fakultät Technik und Informatik
der Hochschule für Angewandte Wissenschaften Hamburg

in Zusammenarbeit mit Firma:
Autoliv B.V. & Co. KG
Abteilung ANG/ES
Otto-Hahn-Straße 4
25337 Elmshorn

Erstprüfer: Prof. Dr.-Ing. Gunnar Simon Gäbel
Zweitprüfer: Dipl.-Ing. Enno Witfeld

Eingereicht am: 30.01.2017

Zusammenfassung

Name des Studierenden
Milan Koch

Thema der Arbeit
Akustiksimulation im Zeitbereich mit Auralisation

Stichworte
Akustik, Auralisierung, Hörbarmachung, huygenssches Prinzip, transiente Simulation, FEM, BEM, Experiment, Validierung, Hörbarmachung, Methodenentwicklung, Signalverarbeitung

Kurzzusammenfassung
Der Gesamtgeräuschpegel von Fahrzeugen ist in den letzten Jahren kontinuierlich gesunken. Durch diesen reduzierten Geräuschpegel ist die Maskierung von Komponentengeräuschen häufig nicht mehr gewährleistet und die akustische Auslegung gewinnt in der Fahrzeugentwicklung immer mehr an Bedeutung. Jedoch sind akustische Tests in der Regel sehr zeitintensiv, teuer und besonders in frühen Entwicklungsphasen sehr aufwändig. Deswegen werden immer häufiger mit Hilfe von Simulationen sogenannte Auralisierungen durchgeführt- d.h. Simulationsmethoden werden verwendet, um Geräusche, unabhängig von Experimenten, hörbar zu machen. In diesem Zusammenhang wird in dieser Arbeit eine Methode entwickelt, um dynamische (FE-)Simulationen im Zeitbereich mit einer Auralisierungs-Methode hörbar zu machen. Dazu können die meisten der kommerziellen FE-Software-Pakete verwendet werden. Die erzeugten Daten der Simulation werden mit einem, in der Arbeit programmierten Skript und mit Hilfe von Signalverarbeitungsverfahren zu einem hörbaren Ergebniss verarbeitet. Um gute Rechnenzeiten des Skripts zu gewährleisten, werden Vereinfachungen wie z.B. das Prinzip der Modalen Superposition oder das Huygensche Prinzip verwendet. Im Laufe dieser Arbeit wird diese Methode auf einige Beispiele angewendet und mit Hilfe eines Experiments validiert. Die Ergebnisse der Beispiele und insbesondere der Validierung sind sehr vielversprechend bezüglich der realitätsnähe, der einfachen Anwendung der Methode und der kurzen Berechnungszeit.

Name of Student
Milan Koch

Title of the paper
Transient Acoustic Simulation with Auralization

Keywords
acoustics, auralization, Huygens' Principle, transient simulation, FEM, BEM, experiment, validation, method development, signal processing

Abstract
Mitigation of interfering noises (e.g. rattling) have become evident in the development of cars due to the continuous reduction of car noise levels in the last years and the resulting masking effect reduction. Therefore, the acoustic requirements for every part of a car have become more important. Physical acoustic tests are time consuming, complex, expensive and in early development phases it is often not possible due to the lack of a prototype. Through the latter reasons simulation tools for the evaluation of acoustic characteristics can be a promising alternative. In this work a procedure is developed to make transient dynamic simulation data audible. The simulation results, which can be generated with most of the commercial FE software, will be processed to an audible result by an auralization method. For an enhanced computational performance simplifications like modal superposition and Huygens' Principle are applied. Within this work, the method has been positively validated by a comparison of simulation to experimental results. The positive validation, combined with the computational efficiency, makes the developed auralization method a promising alternative for the acoustic evaluation of new designs.

Acknowledgements

First of all, I would like to thank my thesis advisor Prof. Dr. Gunnar Gäbel of the Hamburg University of Applied Science. The door to Prof. Gäbel's office was always open whenever I had a question about my research or writing. He consistently allowed this paper to be my own work, but steered me in the right direction whenever he thought I needed it.

I would also like to thank my second thesis advisor and industrial mentor Enno Witfeld. He continuously supported my work and helped me with a lot of essential discussions to find the right direction.

Furthermore I would like to thank Dr. Zhen Wu for his generous support in all manners. He shared his extensive knowledge about acoustics and dynamic simulations with me and supported me in the development of this method.

Thanks to the whole ES/EE department of Autoliv with a special thank to Dr. Burkhard Eickhoff, Dr. Peter Blohme, Christian Kapsalis and Peter Szigeti.

Thanks to everyone involved in this project for the great display of interest in the topic.

Contents

List of Figures

List of Tables

List of Symbols and Abbreviations

Latin Symbols

A_w	Amplitude of wave
A	Area of surface element in m^2
a	Filter coefficient for DC-Blocking filter
a_n	Amplitude and phase of sine wave
a_0	Mean value of signal
b	Width of rectangular pulse in the time domain
b_n	Amplitude and phase of cosine wave
c	Sound velocity in m/s^2
$c_{critical}$	Critical damping
c_d	Damping
$ERP_{absolute}$	Equivalent radiated power in W
ERP_ρ	Equivalent radiated power density in W/m^2
F	Force in N
f	Frequency in Hz
f_c	Cut-off frequency in Hz
f_h	Nyquist frequency in Hz
f_s	Sampling frequency in Hz
g	Gravity in m/s^2
H(f)	Frequency Response Function
h_{total}	Height of vibraphone in m
$h_{resonator}$	Height of resonator in m
I	Impedance in W/m^2
I_{fp}	Impedance at field point in W/m^2
k	Wavenumber
k_s	Spring stiffness in N/m
L	Length of resonator in m
m	Mass in kg
n	Index number of frequency (n=0,1,2,...,n)
$\vec{n}$	Unit vector normal
p	Sound pressure in Pa
p_{max}	Maximum sound pressure in Pa
p_{rms}	Effective (rms) sound pressure in Pa
p_{fp}	Sound pressure at field point in Pa
p_s	Sound pressure of surface element in Pa

$p_{rms,fp}$	Effective (rms) pressure at field point in Pa
$p_{rms,s}$	Effective (rms) pressure of source in Pa
r	Radius in m
r_{s-fp}	Distance between surface element and field point in m
T, T_p	Time of one period in s
t	Time in s
t_{bar}	Thickness of vibraphone bar in m
t_{wall}	Thickness of resonator wall in m
V(r,t)	Kirchhoff's integral theorem
v_n	Surface normal velocity in m/s
$\vec{v}$	Velocity vector in m/s
W_{fp}	Acoustic power at field point in W
W_s	Acoustic power of one surface element in W
w_{total}	Width of vibraphone in m
X(f)	Fourier series in frequency domain
X(k)	Discrete Fourier Transformation of a finite length in frequency domain
x(n)	Discrete Fourier Transformation of a finite length in time domain
x(t)	Fourier series in time domain
z	Specific or characteristic acoustic impedance (wave resistance) in Pa · s/m

Greek and Other Symbols

Δ	Time interval in s
ζ	Damping ratio
λ	Wave length in m
ρ	Density of air m^3/kg
$\varrho(t)$	Envelope function
Φ	Velocity potential
φ	Angle of sound radiation in rad
ω	Angular frequency in 1/s
ω_n	Natural angular frequency in 1/s
ω_w	Resonance angular frequency in 1/s
∇^2	Laplace operator

Abbreviations

BC	**B**efore **C**hrist
BEM	**B**oundary **E**lement **M**ethod
DFB	**D**eformable **R**igid **B**ody
DFT	**D**iscrete **F**ourier **T**ransform
DOF	**D**egrees **O**f **F**reedom
FEM	**F**inite **E**lement **M**ethod
FFT	**F**ast **F**ourier **T**ransformation
FRF	**F**requency **R**esponse **F**unction
FT	**F**ourier **T**ransformation

1 Introduction

Increased customer expectations of acoustics have been addressed to the automotive industry in the last decades which have led to extensive acoustic research and development of e.g. quieter engines and optimized sound absorptions. These efforts result in a significant reduction of the overall sound level which eliminates acoustic masking effects and interfering noises of parts are not covered any longer. In order to increase customer comfort, interfering noises in the vehicle interior need to be avoided and to realize this the acoustic behaviour of every part needs to match the design requirements. Therefore, it is of key importance to evaluate a real sound in order to get an acoustic feeling of a certain situation. A common traditional way to detect acoustically problematic areas of cars is to perform experiments. Though acoustic experiments are expensive, time consuming and the required parts are often not available in early development stages. Therefore, it is promising to increase the utilization of auralization techniques. Auralization describes methods to generate sound from discrete numerical data. Discrete data can be generated with dynamic simulations and made audible with an auralization technique. This gives the possibility to analyse in an efficient way the acoustic effects of design changes in e.g. the geometry of a part. (Oppenheim et al. 2008); (Vorländer 2008)

At the market a handful of commercial software packages are available to perform acoustic simulations with auralization but either the software is inherently expensive or very complex. Therefore, such software packages are not as often used as e.g. deformable FE simulation methods, which are more affordable and more known. In this context, this work presents an approach to make transient simulations with an auralization technique audible. For the transient simulation can be used most of the commercial FE software and the developed auralization technique is performed by scripts with signal processing tools.

The next chapter presents an overview of acoustics and explains the applied acoustic theory within this work.

2 Fundamentals of Acoustics

The word ”acoustic” comes from the Greek word *akoyein* and means ”to hear”. It is the science of sound and its propagation. In one of the first known scientific discussions on acoustics the ancient Greek philosopher Pythagoras analysed the sound impression of stringed instruments in 550 BC. Aristotle figured out later, that sound is a compression and a decompression of air. Around the year zero, Roman architects applied their basic understanding in architectural acoustics to build theatres. In the mid of the 16th century, Galileo Galilei dealt with vibrations and postulated that body vibrations generate waves. From this time the research in acoustics has increased rapidly through e.g. Newton's mathematical description of waves, Lord Rayleigh's postulation of sound theory[1] or Helmholtz's general mathematical description of waves. Furthermore, the electrification, especially induced by Ohm, Faraday and Henry, increased and simplified acoustic research due to various analogies between both fields. With the burgeoning electrification new acoustic technologies got invented, e.g. telegraph techniques or the telephone by Bell and Edison. In the 20^{th} century a new level of precision of acoustic technologies was reached especially through intensified research in war time. During the first quarter of the 20^{th} century an application was developed to detect ultrasonic waves in air and water. Ultrasonic sonic waves describe the frequency range above the human hearing range of 20000 Hz. Especially for medical purposes ultrasonic technologies are very useful. In the early life of a human being a hearing range from 16 Hz to 20000 Hz is normal but the upper level decreases with age. Frequencies below 16 Hz are called infrasound. Acoustic science covers only the human hearing range and is further discussed in the next chapters. (Rossing 2014); (Blauert 2005); (Mach 1919)

2.1 What is Sound?

From the early stages it was known that sound propagates somehow from one point to another. Aristotle postulated that sound propagates through a motion of air. Later, in the 16^{th} century, Galileo Galilei stated that sound waves are generated by vibrations and it has become evident

[1] *The Theory of Sound* is a textbook from Lord Rayleigh and is still used.

that sound propagates by waves in the form of pressure fluctuations. (Rossing 2014); (Mach 1919)

Nowadays, sound is considered to be a mechanical wave in an elastic medium similar to Galileo Galilei's expectation. In liquids and gases, sound propagates in longitudinal waves or so-called "compression waves" because compression stress can be transmitted only (no shear stress). In the latter wave type the particle displacement is parallel to the direction of wave propagation. In solids sound can propagate in longitudinal or transverse waves or in a combination of both. The particle displacement in transverse waves is perpendicular to the direction of wave propagation. (Rossing 2014); (Eichler 2014)

The mathematical description of an acoustic wave propagating in gases or liquids is based on hydrodynamic relations of state changes by relating pressure, particle velocity and density. Since sound propagates by small state changes only, a wave equation can be derived for small changes of states to describe sound fields as a function of time and space. Equation 2.1 shows such a wave equation for the sound pressure p, where ∇^2 describes the Laplace operator[2], c the phase velocity and t the time.

$$\frac{1}{c^2}\frac{\partial^2 p}{\partial t^2} - \nabla^2 p = 0, \tag{2.1}$$

Based on equation 2.1 an expression for the velocity field can be derived by introducing a change in density ρ but writing the wave equation as a function of the velocity potential Φ is most convenient (see equation 2.2) because Φ allows a direct calculation of pressure and velocity. (Lerch et al. 2009); (Eichler 2014)

$$\frac{1}{c^2}\frac{\partial^2 \Phi}{\partial t^2} - \nabla^2 \Phi = 0 \tag{2.2}$$

Additional to pressure and velocity changes, for the analysis of acoustic behaviour it is of key importance to consider the wave propagation, here historically named as Huygens' Principle.

2.2 Huygens' Principle

In 1678 in France, the Dutch mathematician and scientist Christiaan Huygens (*1629 – †1695) finishes his first version of *Traité de la lumière (engl. Treatise on Light)*. This work is the first

[2]The Laplace differential scalar operator can be applied to vector or scalar fields: $\nabla^2 = \partial^2/(\partial x^2) + \partial^2/(\partial y^2) + \partial^2/(\partial z^2)$. (Lerch et al. 2009)

mathematical theory of light. During the following 12 years he continuously discusses and improves the content with scientists of the Royal Academy of Science and publishes the treatise in 1690. (Huygens 1690)

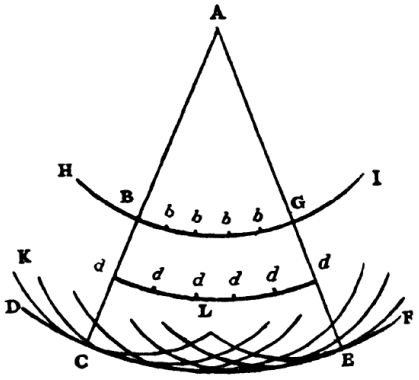

Figure 2.1: Huygens principle of wave propagation (Huygens 1690, p. 19)

For the first time in this textbook Huygens considers light to be a wave and outlines the rectilinear wave propagation of point sources. By means of figure 2.1 Huygens depicts that every point of a wave front is the initial point of a new wavelet, whose envelope creates a new wave front with the same frequency and phase as the previous wave. (Huygens 1690); (Veselov 2002)

Precisely, point "A" is a point source, which creates the spherical wave front "H-I". According to Huygens' Principle any point of this wave front is the initial point of a wavelet, whose envelope represents the new wave front "D-F". Later, in 1816 the French physicist and engineer Augustin Jean Fresnel (*1788 – †1827) describes diffraction on edges and apertures with Huygens' Principle by including the superposition principle for the amplitudes of the secondary waves. The result of his work is known as Huygens Fresnel Principle. (Veselov 2002)

However, Huygens and Fresnels theories do not describe properly wave propagation in free space, especially because of the negligence of backward waves. The German physicist and physician Hermann L.F. von Helmholtz (*1821 – †1894) is the first to take backward waves for longitudinal, monochromatic[3] waves into account in the so-called Helmholtz wave equations. Helmholtz wave equations are partial differential equations, which expresses a time-independent form of the wave equation (equation 2.1):

$$\nabla^2 \cdot A_w + k^2 \cdot A_w = 0, \tag{2.3}$$

[3] A monochromatic wave consists of a narrow band of wavelengths.

where ∇^2 describes the Laplace Operator, A_w the amplitude and k the wavenumber[4]. (Born & Wolf 2003); (Eichler 2014)

Later, the German physicist Gustav Kirchhoff (*1824 – †1887) enhances Helmholtz theory for longitudinal waves further to a more general theory of wave propagation by using Maxwell-Equations[5] and Green's identities[6] to describe mathematically exact the Huygens Fresnel Principle of wave propagation in the so-called Kirchhoff's integral theorem[7]. (Miller 2010); (Wrobel 2002)

$$V(r,t) = \frac{1}{4\pi} \int_S \left\{ [V] \frac{\delta}{\delta n} \left(\frac{1}{s} \right) - \frac{1}{cs} \frac{\delta s}{\delta n} \left[\frac{\delta V}{\delta t} \right] - \frac{1}{s} \left[\frac{\delta V}{\delta n} \right] \right\} dS, \tag{2.4}$$

Equation 2.4 shows the Kirchhoff's integral[8] for non-monochromatic waves. This equation is commonly used to calculate sound in the far field at an arbitrary point. Schönwald (2010); Goodman (2005); Born & Wolf (2003)

However, knowing the wave propagation and the pressure or velocity change in a certain situation is not enough to describe and evaluate acoustic behaviour. Additionally, it is necessary to consider the anatomy and the hearing capabilities of the human ear as well.

2.3 Human Hearing

A human ear consists basically of an outer ear, a middle ear and an inner ear (see figure 2.2). Firstly, pressure changes (sound) from the environment are captured by the outer ear depending on frequency and direction. Secondly, the middle ear transfers the sound from outer ear to inner ear and basically, it fixes the impedance and the ear drum responses frequency dependent. Thirdly, the inner ear transforms the mechanical wave into stimuli, which are distributed to the sensory cells.

This transformation happens in the so-called basilar membrane, a part of the cochlea. Furthermore, the mechanical properties of the cochlea varies in the length (uncoiled state) due to the change of its thickness from 1/6 mm to 1/2 mm. This is why different frequencies excite different areas and amplitudes of the Cochlea. This behaviour is summarized in the

[4] The wave number is the quotient of angular frequency ω and speed of light c: k = ω /c.

[5] The Maxwell-Equations are four partial differential equations, which describe the behaviour of electric and magnetic fields.

[6] Green's identities are named after the British mathematical physicist George Green (*1793 – †1841) and it is known as conclusion of the divergence theorem. It consists of three derivative and integral vector identities.

[7] The Kirchhoff's integral theorem is sometimes refereed as Fresnel-Kirchhoff integral theorem.

[8] For further information to Kirchhoff's integral theorem and its derivation is refereed to Goodman (2005) and Born & Wolf (2003).

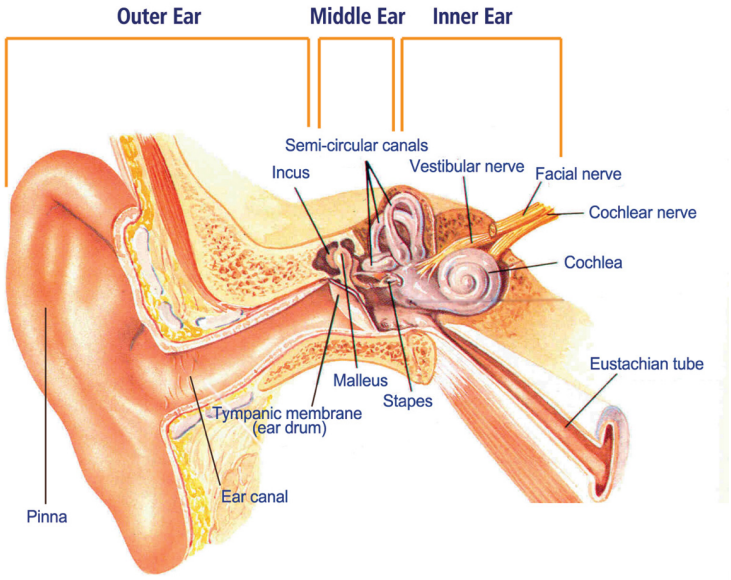

Figure 2.2: The anatomy of the human ear (The Art of Hearing 2014)

travelling wave theory, which says that the hearing capabilities of the human ear are frequency dependent. Moreover, the perception of acoustic waves in the sensory cells depends not only on frequency but also on different sound pressure levels, which is illustrated in the equal-loudness contours (see figure 2.3). The y-axis represents the sound pressure level in dB and the x-axis shows the frequency in Hz. (Wendt 2016)

Generally, the frequency dependency of the sound pressure level is the foundation for evaluated acoustic measurements: the A-weighting is a commonly used filter in acoustic measuring techniques and represents the sensed sound pressure level of humans depending on frequency. (ISO EN 226:2003 2014); (Wendt 2016)

However, a pure analysis of acoustic curves is often not a targeted approach to analyse acoustic behaviours because not all characteristics can be captured. Therefore, it is often convenient to evaluate sounds by humans through listening in order to get information of how humans feel about certain sounds. This approach is summarized in the acoustic discipline psychoacoustics.

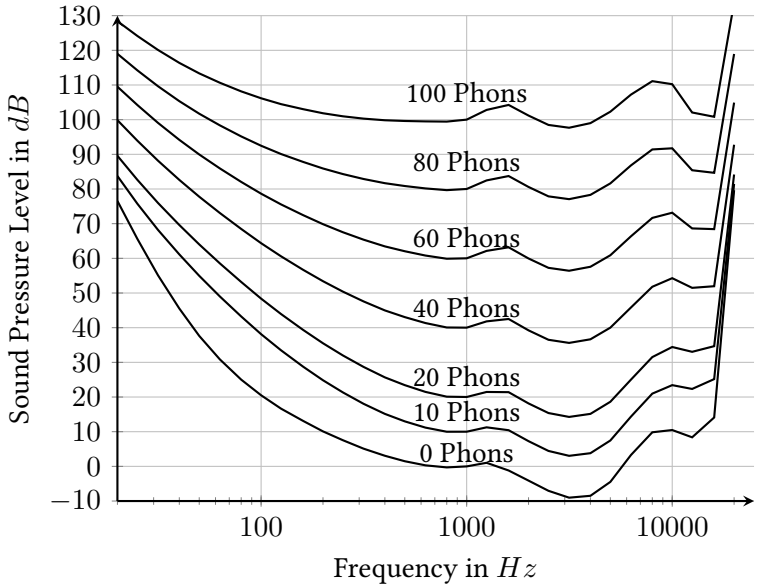

Figure 2.3: Equal-loudness contours acoording to ISO EN 226:2003 (2014)

2.4 Psychoacoustics

Psychoacoustic assessments are mainly used to investigate the human sound impressions. Generally, acoustic waves act as stimuli on the basilar membrane which, transforms stimuli into human perceptions. The properties of an acoustic wave can be clearly defined with physical quantities. In comparison the human perception is subjective and differs from human to human and is therefore difficult to determine. According to DIN 55350-11:2008-05 (2008) sound quality is defined as satisfaction of the expectations. That means that humans expect certain sounds in certain situations, e.g. a sound when buckling up: this sound generates safety feelings for humans and is expected. In case of a silent buckling up, customers will not be satisfied. Furthermore, altering sound emissions and thus sound impressions of e.g. cars offers a possibility to communicate the product value: a low-frequency dull door closing sound seems more high-quality than a tinny sound with higher frequency. Furthermore, the feeling of comfort correlates strongly with undisturbed communication abilities at higher velocities. Therefore, assessments to determine sound impressions with clear defined evaluation criteria like ”Zwicker” or the ”Annoyance Index” are carried out. For each evaluation criteria several perception variables are defined in order to evaluated the entire sound impression. (Zeller 2012); (Braess & Seiffert 2013)

Traditionally psychoacoustic researches and generally acoustic studies are done with experiments and assessments. Nowadays, techniques are available to make specific situations audible by using simulations in order to avoid running expensive and time consuming experiments. In this context, the next chapter shows commercial acoustic simulation techniques.

3 Acoustic Simulation Methods

This chapter presents an overview of methods and software packages for acoustic simulations. These numerical simulation approaches can be grouped by their domain: time or frequency. The time domain is widely used for e.g. deformation calculation and regarding acoustics, the time domain is especially a good choice if the target is to provide audible results (auralization). The frequency domain is usually a good choice if frequency information and system characterisitics are needed. Most of the commercial software companies offer different software packages depending on the specific problem for simulating in the time- or frequency domain, whereby in the field of acoustics, the most widely used methods are the so-called Finite Element Method (abbr. FEM) and the Boundary Element Method (abbr. BEM). FEM and BEM are commonly used i.a. for acoustic calculations because many traditional structure solvers include these methods e.g. the software 'Abaqus' (FEM) from 'Dassault Systèmes' or 'LS-DYNA' (FEM and BEM) from 'Livermore Software Technology Corporation'. These methods are based on classical dynamic simulations and use traditionally the frequency domain. In case of the BEM the so-called Sommerfeld radiation condition[1] is automatically satisfied, that means that the exterior domain does not need to be meshed. (Huang & Cui 2013); (Vorländer 2008); (Chandler-Wilde & Langdon 2007); (Dassault Systèmes 2017)

On the right hand side of figure 3.1 is depicted that an air volume (the area between boundary and body) of BEM simulations are not necessarily meshed. This is beneficial regarding the meshing time compared to the acoustic FEM (left hand side), where the whole field has to be discretized.

However, FEM simulations are often used to visualize the wave propagation in the medium and BEM simulation are more commonly performed to calculate the behaviour at the boundary points only, or in the so-called indirect BEM simulations at single boundary points, which can be advantageous for a fast meshing procedure. Figure 3.2 depicts on the right hand side an indirect BEM simulation, which can calculate interior and exterior problems in the so-called

[1] Arnold Sommerfeld (*1868 – †1951) was a German theoretical physicist. He discovered the condition of radiation for scalar fields by satisfying the Helmholtz equation (see equation 2.3). With Sommerfeld's approach the Helmholtz equation can be solved uniquely. For further information about Sommerfeld's radiation is referred to Ammari (2008).

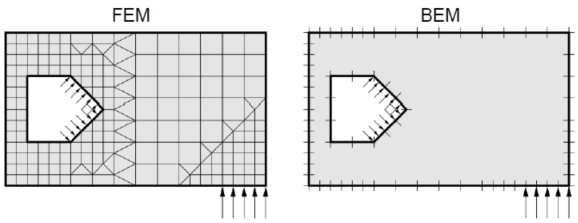

Figure 3.1: The simulation methods FEM and BEM (Gaul et al. 2003)

open and closed domain. Whereas a direct BEM simulation (left hand side) is used for closed domains only, that means either for interior or exterior problems. (Chandler-Wilde & Langdon 2007); (Huang & Cui 2013)

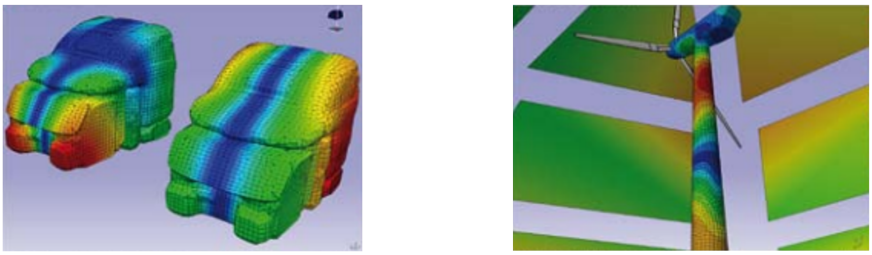

Figure 3.2: The direct (left) and indirect (right) BEM (according to Siemens AG (2017))

Also the Finite Element Method has advantages compared to BEM especially regarding calculation time, because the matrices are not fully populated and they do not need to be reformed at each frequency. However, both methods have advantages and disadvantages and which method is beneficial depends on the specific problem. (Chandler-Wilde & Langdon 2007)

A BEM simulation of a vibraphone bar has been carried out within this work with 'LS-DYNA' which is illustrated in figure 3.3. The vibraphone (blue) is a musical instrument, which basically consist of a bar and a resonator. It is usually excited in the middle point on the top of the bar by a mallet. The mesh above the vibraphone depicts the field at 880 Hz with the unit sound pressure level in decibel (dB). According to figure 3.2, this is an indirect BEM simulation due to the open domain. For more detailed information about this BEM simulation it is referred to chapter 5.4.3.

The frequency domain simulation methods FEM and BEM can be used to calculate e.g. the sound pressure level as function of frequency at a field point. Furthermore, they can be used to visualize the sound propagation of a body (see figure 3.3). Nowadays, it is becoming more evident to generate realistic audible sound from simulation data instead of analysing

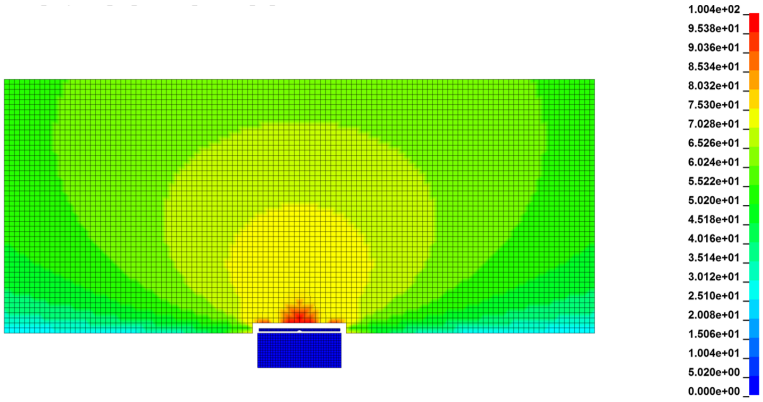

Figure 3.3: A BEM simulation of a vibraphone bar carried out with the software 'LS-DYNA'

frequency curves. In this context, auralization describes the process of making numerical data from simulations audible. This technique simplifies acoustic studies because it is possible to listen to close to reality synthesized sounds and to evaluate its characteristics according to the psychoacoustics (see chapter 2.4). Thus, auralization together with psychoacoustics build a strong tool to analyse acoustics of a product or a part before a prototype has been build. It is especially suitable to analyse acoustics regarding customer comfort. Since auralization happens mostly in the time domain it is more convenient to perform simulations directly in the time domain and not in the frequency domain. Whereupon, a convolution of data from the frequency domain to the time domain is possible but such universe transformations are valid for small changes in the energy level only, which mostly do not occur in acoustic problems (see chapter 4.1). Therefore, it is more common to simulate directly in the time domain in order to avoid a problematic transformation. E.g. the software 'LMS Virtual.Lab' from Siemens offers to simulate acoustic BEM or FEM in the time domain and to visualize sound propagation in time. However, these two time domain methods are usually performed for small frequency ranges only due to the large computational effort. Therefore these methods are not suitable for auralization purposes. A more common approach to generate sound from simulation is to track each ray: 'Ray Acoustics' from 'Siemens' represents a ray tracing method, which is performed in the time domain. This allows to calculate sound propagation in a range of frequencies up to 18000 Hz in the far field, whereby the calculation follows the track of each ray of sound while reflection, absorption etc. is taken into account. Furthermore, ray tracing simulations are often supported by FEM and BEM in order to e.g. pre-calculate the radiation characteristics of the sources properly. (Siemens AG 2017); (Vorländer 2008)

In this chapter a brief overview of the wide range of acoustic simulation methods and its combination has been presented. The shown methods represent the fundamental basis of many acoustic simulation methods and its commercial use. The software companies often combine different simulation methods in order to use the advantage of each technique, e.g. the combination of FEM or BEM methods with the ray tracing technique. This approach is in line with the objective of this work: on the basis of structural dynamic simulation data a kind of ray tracing method is to develop to make simulation data audible, whereby the support of BEM simulations is to estimate. To develop an own procedure has advantages compared to most commercial software packages: on the one hand side buying expensive acoustic software can be avoided and on the other hand side the use of structural dynamic simulation data enlarges huge advantages because this data is existing in most technical developments anyway, or otherwise it can be created with the common dynamic simulation tools.

In order to process numerical simulation by an auralization method, it is important to take signal processing into account, which is discussed in the next chapter.

4 Discrete-Time Signal Processing

Signal processing has a long history from the 17^{th} century, when scientists and engineers started working intensively on functions with continuous variables and differential equations. A continuous (or analogue) function is characterized by an uncountable domain through a continuously changing variable. Most of the natural incidents (e.g. temperature change or seismic measurements) are described by a continuous-time signal. First from the upgrowth of computer technologies in the 1950s it was of key importance to impose a sampling procedure on the continuous signals in order to make data processable by computers. Figure 4.1 depicts the difference between a continuum and a discrete time signal. A digital signal (or sequence) is built upon a set of discrete values, where time is sampled at every Δ seconds. (Do et al. 2012); (Agilent Technologies 2012)

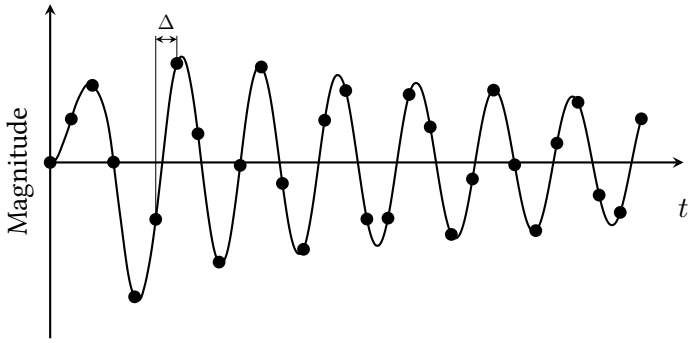

Figure 4.1: A continuous signal (line) sampled at every Δ second to a discrete signal (dots)

The availability of computer provides an extraordinary advantage for data processing in terms of flexibility: as one of the pioneers, in the early 1950s, oil companies used digital discrete-time signal processing tools and stored seismic data on magnetic tapes for later processing. From this moment the role of signal processing has expanded significantly in a wide range of fields from specialized military systems, telecommunication systems, space explorations, medicine technologies, industrial applications and video and photo editing. (Do et al. 2012); (Agilent Technologies 2012); (Chen 2007)

Signal processing describes a procedure used on measured data. A signal carries physical information like temperature, acceleration or pressure. On these information a series of steps or operations will be applied, so-called processing, to modify, manipulate or transform the signal by a system to make data better understandable, interpretable and processable without changing desired characteristics. Basically, signal processing tools are used when it seems difficult to extract information from a signal through direct observations. (Shin & Hammond 2007); (Do et al. 2012); (Agilent Technologies 2012)

A common way to describe the process of a signal processing task is by using system block diagrams. Figure 4.2 depicts the relation between activator x(t) (or independent variable) and response function y(t) (or dependent variable). (Shin & Hammond 2007)

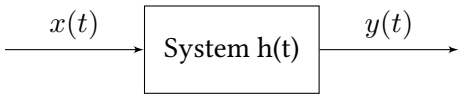

Figure 4.2: Definition of a linear system

The activator represents the input signal, which is processed in a linear system h(t) in order to calculate y(t). Mathematically, the system above can be expressed by y(t)=h(t) · x(t), where the dot is the convolution integration. (Shin & Hammond 2007)

In order to understand a system more in detail, it is often recommended to analyse the input-output relationship of x(t) and y(t). Therefore, a common way to identify a system, is to use the frequency information of x(t)->X(f) and y(t)->Y(f) in order to calculate the Frequency Response Function (abbr. FRF) H(f), which represents in acoustics the so-called acoustical sensitivity:

$$H(f) = \frac{Y(f)}{X(f)}. \tag{4.1}$$

The great advantage of FRF is that different tests of a linear system can be easily compared with each other. Basically, H(f) is a complex quantity and consists therefore of real and imaginary components, which can be separately depicted in the amplitude (real) and the phase (imaginary) diagram. Figure 4.3 depicts the real part[1] of H(f) of an experimental run with a force as input to excite a system and a measured sound pressure level in dB at one certain point in the field as output. Therefore, the magnitude of this FRF is defined by sound pressure level/force in the frequency domain. The two peaks indicate the resonance frequencies of the system. (Shin & Hammond 2007); (Oppenheim et al. 1989)

[1]For this work the phase diagram does not provide more comprehensibility and is therefore not depicted.

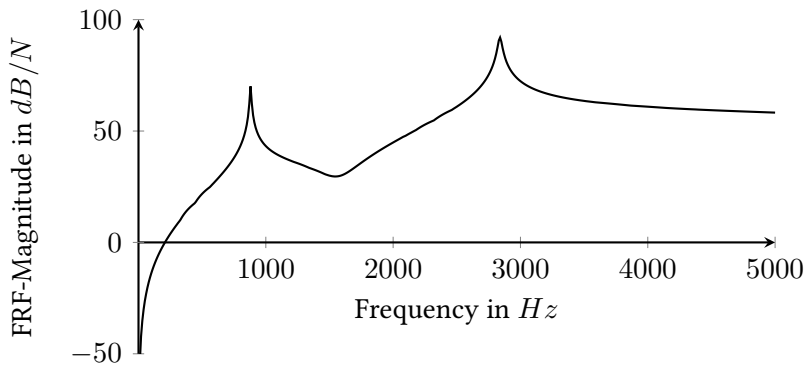

Figure 4.3: The amplitude of the acoustic sensitivity (FRF)

The most traditional way to observe a signal is over time (in the time domain). Nevertheless, it is often challenging to understand and to interpret signals in this domain. Moreover, it is of key importance to change the perspective and transform a signal from the time domain to the frequency domain. A common transformation to convolute signals is to use the Fourier Transformation (abbr. FT).

4.1 Fourier Transformation

In 1807 Jean Baptiste Joseph Fourier, a French mathematician and physician, postulates that an infinite linear combination of harmonic waves can build up any periodic signal. To give an illustration, figure 4.4 shows on the left hand side a harmonic wave $\sin(2\pi x) + \frac{1}{2}\sin(6\pi x)$, which consists of the two harmonics on the right hand side.

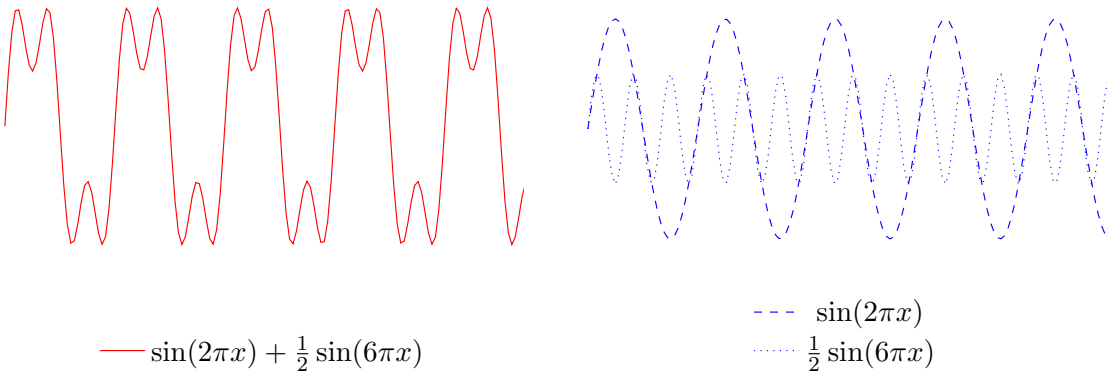

Figure 4.4: The decomposition of a periodic signal (left) with harmonic sinusoidal waves (right)

The harmonic waves are illustrated by $sin(\omega t+\varphi_0)$, where ω describes the angular frequency with

$$\omega = 2\pi f = \frac{2\pi}{T} \tag{4.2}$$

and φ_0 the phase, which is zero in this example. Hence, knowing the harmonic composition of a signal and applying equation 4.2 allows an easy detection of the frequency components: the dashed curve on the right hand side of figure 4.4 ($\sin(2\pi x)$) has an angular frequency of $\omega = 2\pi$, that means a frequency of f_1= ω / 2 π = 2 π / 2 π = 1 Hz. Thus, the dotted curve (1/2 $\sin(6\pi x)$) has a frequency of f_2=3 Hz. Figure 4.5 illustrates the frequencies and their time domain information in a so-called waterfall plot.

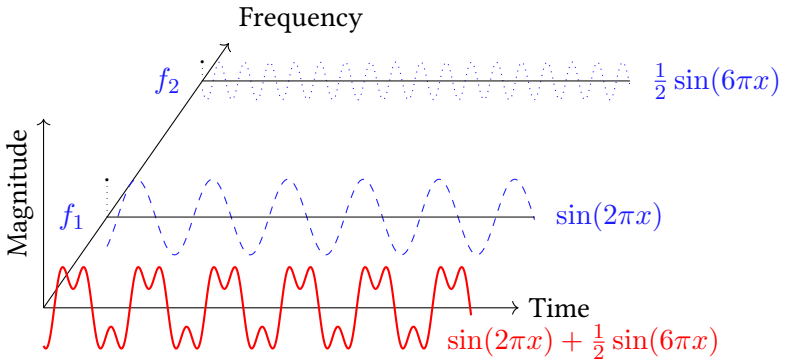

Figure 4.5: The waterfall plot depicts the relationship between the time- and frequency domain

As depicted, each harmonic component of a signal represents one frequency contained in the signal. Rotating the view on the plot of figure 4.5 to frequency as x-axis and magnitude as y-axis will lead to the following discrete frequency spectrum:

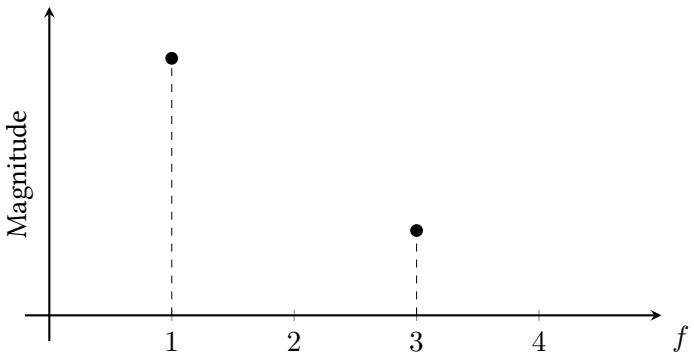

Figure 4.6: The frequency spectrum of $\sin(2\pi x) + \frac{1}{2}\sin(6\pi x)$

Basically, a frequency spectrum provides deeper information compared to the signal in the time domain: it is used to analyse the behaviour of a system in order to identify its intrinsic frequency characteristics. (Agilent Technologies 2012); (Do et al. 2012); (Shin & Hammond 2007)

Real measured signals are generally much more complex than the example above (see figure 4.4). For this reason, it is not feasible to identify the frequency components manually. To transform more complex signals, Fourier has developed methods to convolute a signal from the time domain to the frequency domain and inverse. These methods are based on the introduced concept of decomposing a signal into a sum of "simpler" components. The first way to get the frequency information of a signal is by applying the Fourier Series. Equation 4.3 shows the Fourier Series for a continuous periodic signal with the period length T_p,

$$x(t) = \frac{a_0}{2} + \sum_{n=1}^{\infty} \left[a_n cos\left(\frac{2\pi nt}{T_p}\right) + b_n sin\left(\frac{2\pi nt}{T_p}\right) \right], \tag{4.3}$$

where a_0 / 2 determines the mean value of the signal. The amplitude and phase of each sine and cosine wave is represented by a_n and b_n, respectively. Furthermore, the fundamental frequency is f_1 = 1 / T_p and the other frequencies are concerning n=1,2,... multiples of this. Figure 4.7 depicts the partial sums of the applied Fourier Series on a square wave, where a_0=0, a_n=0 and b_n= 2 / (n π)) · (1-$cos(n\pi)$). It can be observed, that just sine waves and odd functions have to be considered to build up this square wave. (Shin & Hammond 2007)

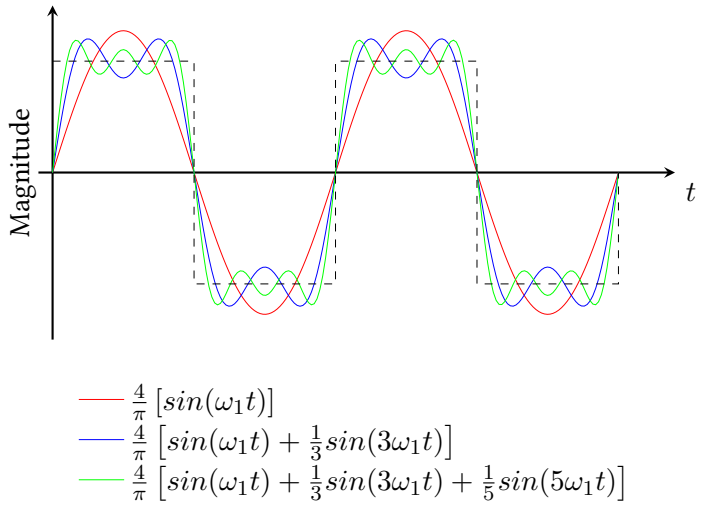

Figure 4.7: Fourier Series applied on square wave

In this context Gibbs'[2] Phenomenon states that there will be a significant error in the vicinity of a discontinuity when applying Fourier Series on a function. In other words, it does not matter how many partial terms are applied in equation 4.3, there will still be an error. This can easily be observed, for instance, on the shown square wave example: as depicted, the linear combination of sine waves is not sufficient to represent the square waves properly. In the vicinity of the discontinuities of the linear combinations an overshoot will appear. (Shin & Hammond 2007); (Do et al. 2012); (Agilent Technologies 2012)

Applying a basic Fourier Series on a function leads to a discrete spectrum because the frequencies are only multiplies of the smallest chosen frequeny or the fundamental frequency. Figure 4.8 shows the spectrum of the square wave with a distance between the frequencies of f=1 / T_p. Furthermore, the frequencies of all even functions are zero due to b_n= 2 / (n π) (1-$cos(n\pi)$). (Shin & Hammond 2007)

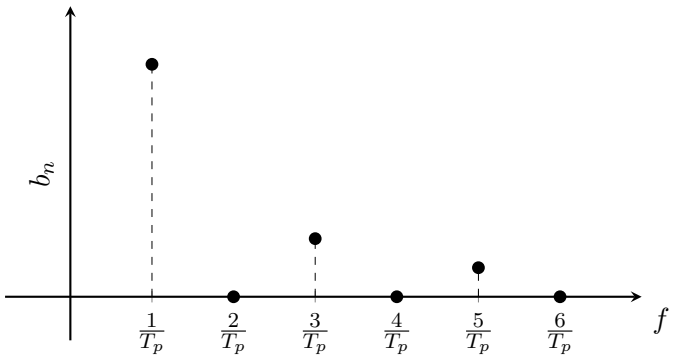

Figure 4.8: Frequency spectrum of applied Fourier Series on square wave

However, the behaviour of most real signals are not characterized by discrete spectra but rather by continuous frequency spectra. Hence, Fourier has extended the Fourier Series to convolute time series into a continuous frequency domain. Therefore, it is convenient to take the complex form of the Fourier Series by using $e^{\pm j2\pi f}$ into account in order to derive the continuous Fourier Integrals (or the true Fourier Transforms) which may be expressed by:

$$x(t) = \int_{-\infty}^{\infty} X(f)e^{-j2\pi ft}df \; and \; X(f) = \int_{-\infty}^{\infty} x(t)e^{-j2\pi ft}dt. \tag{4.4}$$

[2]Josiah Willard Gibbs (*1839 – †1903) was an American scientist.

This procedure is called Fourier Transformation (abbr. FT). For instance, figure 4.9 shows a transformation of a rectangular pulse function from the time to frequency domain by applying the Fourier Integral:

$$X(f) = \int_{-\infty}^{\infty} x(t)e^{-j2\pi ft}dt = \int_{-b}^{b} ae^{-j2\pi ft}dt = \frac{2absin(2\pi fb)}{2\pi fb}. \tag{4.5}$$

The solved integral function in the frequency domain is called sinc function and generally defined by sin(x)/x. Sinc functions are symmetric to the y-axis and $\lim_{a\to\infty} sin(a)/a$ asymptotically tends to zero. The sinc function shown on the right hand side of figure 4.9 represents the spectrum of a rectangular pulse with a width in time of 2b, depicted on the left hand side of figure 4.9, which results in a first zero crossing of 1/(2b) in the frequency domain. (Shin & Hammond 2007); (Oppenheim et al. 1989); (Do et al. 2012)

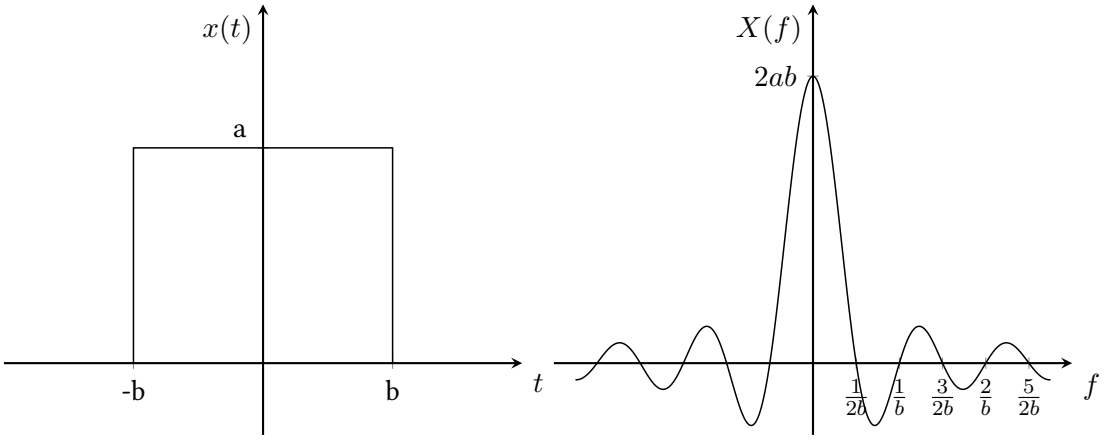

Figure 4.9: The convolution of a rectangular pulse from the time- to frequency domain

However, this approach is considered for continuous functions. For digital data processing it is, as mentioned, indispensable to have discrete data points. In this context another approach to the so-called Fourier Transform (see equation 4.4), namely the Discrete Fourier Transform (abbr. DFT), may be used. The DFT can be derived from the continuous Fourier Transform with the steps described in the following sentences. First a discrete time series can be considered. According to equation 4.4, the area under the curve can be determined for a continuous series. For a discrete signal this can be done by using a sum function coupled with the time interval between samples to calculate separately the area of each time interval in order to sum all areas up. A summation from minus infinity to plus infinity would take infinite time. Hence, a

limitation of the transform is important. This leads to the Discrete Fourier Transformation of a finite length (or periodic) sequence:

$$x(n) = \frac{1}{N} \sum_{k=0}^{N-1} X(k) e^{j(2\pi/N)nk} \; and \; X(k) = \sum_{k=0}^{N-1} x(n) e^{-j(2\pi/N)nk}, \tag{4.6}$$

where x(n) is the discrete signal representation of the sampled points n, N the total amount of sampled points n, X(k) the discrete frequency domain representation with f=k/ (N Δ) and Δ describing the time step or the time interval. It is notable to see the relationship of Discrete Fourier Transformation X(k) and Fourier Transformation of a sampled sequence[3] $Xe^{2j\pi f\Delta}$ (Shin & Hammond 2007):

$$X(k) = Xe^{2j\pi f\Delta} \tag{4.7}$$

The main difference between FT and DFT lays within the representation in the frequency domain. The Fourier Transformation of a sampled sequence generates a continuous spectrum in comparison to the Discrete Fourier Transformation, where the spectrum is calculated at discrete data points. Therefore, it is questionable why DFT is used instead of FT. The most persuasive argument for using DFT is the computation time. In this context, Karl Friedrich Gauss (*1777 – †1855), German mathematician and physician, invented an algorithm to interpolate the trajectories of asteroids. This algorithm, nowadays so-called Fast Fourier Transformation (abbr. FFT), was rediscovered in 1965 by Cooley and Tukey[4] and is capable to transform data from the time- to frequency domain (or inverse) in a very effective manner. FFT based on the idea that N is a multiple of two, whereby it allows certain symmetries and can reduce consequently the number of calculation by decomposing the computation of a DFT into smaller DFTs. (Shin & Hammond 2007); (Do et al. 2012); (Agilent Technologies 2012); (Tan & Jiang 2008); (Oppenheim et al. 1989); (Goodman 2005)

These smaller DFTs are applied successively on the signal in order to calculate the DFT block wise. The signal data of one small DFT is called time record. Thereby, the fundamental requirement of the Fourier Transformation is to have an amplitude of zero in the beginning and the ending of the time record. This is normally not fulfilled and therefore a so-called window with zero amplitudes in the start and end points is applied. The window function should always be chosen carefully concerning the character of a certain signal in order to capture all signal components. Therefore, the time records are mostly overlapped to avoid

[3] The Fourier Transformation of a sampled sequence can be derived from the continuous Fourier Integrals (see equation 4.4 The detailed derivation is shown in (Shin & Hammond 2007).

[4] James W. Cooley and John Tukey were American mathematicians.

loosing information. One of the most common window types are Hamming-, Hann- or the based cosine-window. (Shin & Hammond 2007); (Do et al. 2012); (Agilent Technologies 2012); (Oppenheim et al. 1989)

Considered the fact that the frequency domain is discrete when FFT is used, it is important to choose the right time interval (Δ) for the specific problem in order to obtain a representative frequency spectrum. Therefore, sampling can be necessary to change the amount of data per unit time prior to a FFT.

4.2 Sampling

Sampling of data is a fundamental method of Digital Signal Processing. Historically, it represents the bridge between analogue and digital data. Nowadays, sampling procedures are widely used to alter the amount of samples of a signal. Thereby, the main purpose of sampling is to archive a reasonable sampling rate f_s for a specific problem. In other words, the amount of data per unit time depends strongly on the specific objective. To give an illustration for the wide range of sampling rates: a television works normally with a sound (sampling) rate of about f_s=48000 Hz and a video frame (sampling) rate of about f_s=100 Hz (frames/s). That means that the requirements for these two purposes differ concerning the hearing and vision capabilities of humans. In order to understand this behaviour it is important to take the sampling theorem into account. Harry Nyquist (*1889 – †1976), an American electronic engineer, postulates in 1928 at first that the sampling rate of a digital signal should be two times greater or equal to the highest frequency containing a continuous signal to capture all signal information. It may be expressed as:

$$f_s \geq 2f_h. \tag{4.8}$$

21 years after Nyquists discovery, Claude Shannon, the so-called "father of information theory", proved the theorem. Nowadays, it is known as Nyquist-Shannon sampling theorem. (Shin & Hammond 2007); (Do et al. 2012); (Agilent Technologies 2012)

All things considered, it seems that a sampling rate for audio of f_s=2f_h=2 $\cdot$ 20000 Hz = 40000 Hz should be sufficient for the human hearing range (16 Hz- 20000 Hz). This is partly true, but the last decades have shown that a sound rate around 50000 Hz is a better choice according to the relation of quality and data usage[5]. Furthermore, sampling rates above 50000-60000 Hz do

[5]Certainly, the filter techniques are not able to cut off the frequency at one specific point, but rather in a frequency band. Therefore, the highest frequency has to be naturally above $2f_h$.

not provide better sound qualities. However, especially from old western movies, the so-called stagecoach effect is known: the wheels seem to turn backwards when going forward. That is happening due to the fact of low sampling rates and is called aliasing. Figure 4.10 depicts the effect of aliasing in the time domain. It can be seen, that for a representative discretization the sampling rate needs to be sufficiently large.

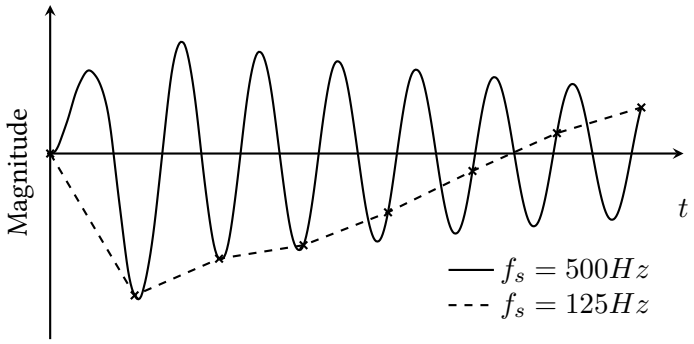

Figure 4.10: Aliasing in the time domain

Therefore, the Shannon-Nyquist sampling theorem of the dashed graph in the example is not fulfilled because the sampling frequency is less than $2f_h$. However, this frequency dependency of aliasing can be better seen in the frequency domain: Figure 4.11 shows a Fourier Transformation of a continuous signal with the condition X(f) = 0 for $|\,f\,| > f_h$. The contour of the frequency content is illustrated as triangle. (Shin & Hammond 2007); (Do et al. 2012)

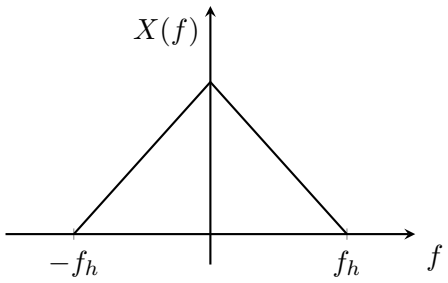

Figure 4.11: Fourier transformation of a continuous signal (according to Shin & Hammond 2007, p. 127)

The sampling rate may be expressed as,

$$f_s = \frac{1}{\Delta}, \tag{4.9}$$

where Δ describes the time interval. This relation coupled with the sampling theorem $f_s \geq 2\ f_h$ leads to the folding frequency:

$$f_h \leq \frac{1}{2\Delta}\ or\ f_h \leq \frac{f_s}{2}. \tag{4.10}$$

According to chapter 4.1 it is known that the Fourier Transformation of a sampled sequence can be expressed as ΔX(f) or $\Delta X(e^{j2\pi f\Delta})$, which is illustrated with $f_s > 2f_h$ in Figure 4.12. Thereby, the highest frequency of the signal f_h is called Nyquist frequency and f_s/2=1/(2 Δ) is the folding frequency. The folding frequency describes the frequency between two subsequent frequency samples. (Shin & Hammond 2007); (Tan & Jiang 2008)

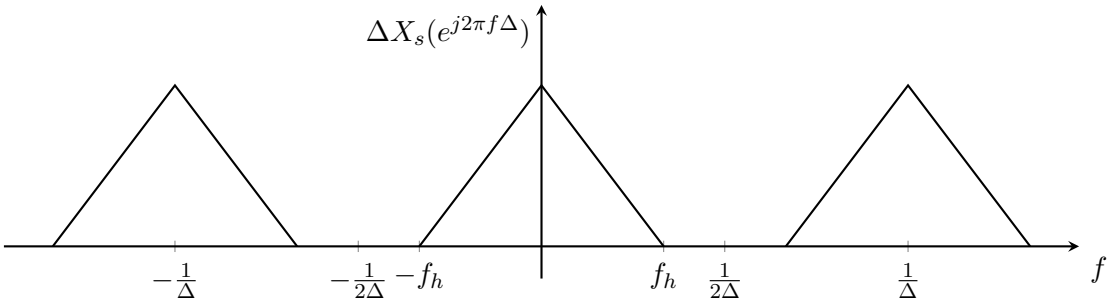

Figure 4.12: Fourier transformation of a sampled sequence, $f_s > 2f_h$ (according to Shin & Hammond 2007, p. 127)

Figure 4.13 represents the case of $f_s < 2\ f_h$. That indicates, that the Shannon-Nyquist theorem is not fulfilled and aliasing can occur.

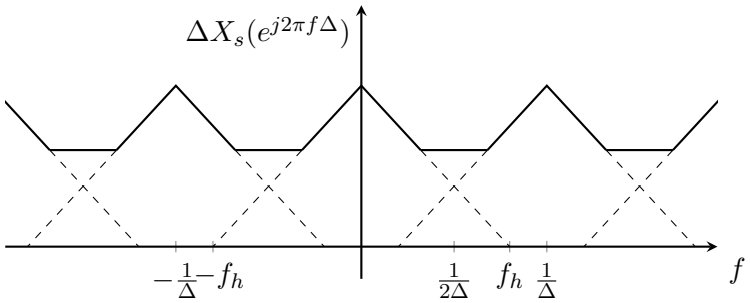

Figure 4.13: Fourier transformation of a sampled sequence, $f_s < 2f_h$ (according to Shin & Hammond 2007, p. 127)

Thus, the frequency functions in X(f) are shifted closer together and overlap in higher frequency areas, which results in a distortion of the frequencies: higher frequencies are not distinguishable from lower ones, which is called aliasing. In other words, sampled frequencies

higher than Nyquist frequency will be interpreted as lower frequency (see figure 4.10). Therefore, it is of key importance to know the highest frequency of the signal in order to define the right sampling rate. Yet the highest frequency of signals is not known and this is why it is recommended to reduce the bandwidth before sampling. A common procedure, depicted in figure 4.14, is to apply a low-pass filter, the so-called anti-aliasing filter and do the sampling procedure afterwards. (Shin & Hammond 2007)

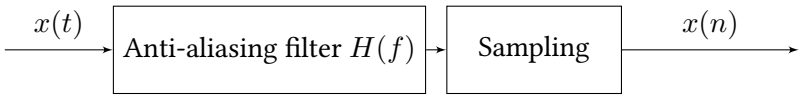

Figure 4.14: Anti-Aliasing filter (according to Shin & Hammond 2007, p. 130)

Low pass filters ramp down high frequencies amplitudes above the cut-off frequency f_c. Figure 4.15 depicts on the left hand side an ideal low pass filter. In this case the highest frequency is equal to the cut-off frequency (f_h=f_c). On the right hand side of figure 4.15 is shown that a real filter has a transition band from f_c to f_h in which the filter gain rises from 0 to maximum. (Shin & Hammond 2007)

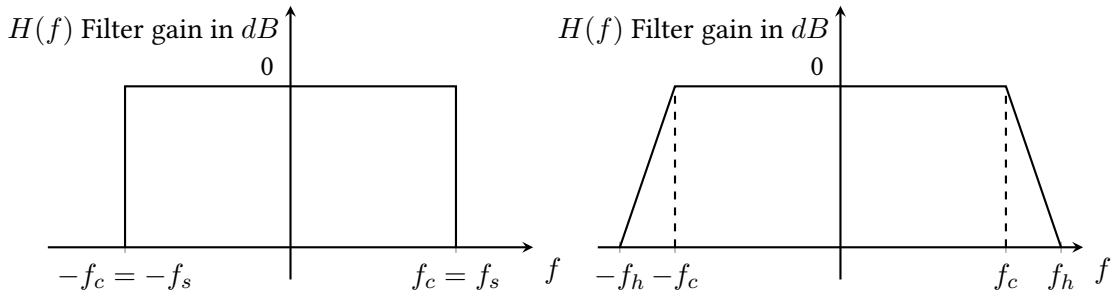

Figure 4.15: Ideal- (left) and real (right) Anti-Aliasing filter (according to Agilent Technologies 2012, p. 31)

In conclusion, the only way to avoid aliasing is to apply an Anti-Aliasing filter. A sampled signal is no longer an exact signal representation but it can be close to reality depending on chosen distance of samples. The appropriate sampling rate is of key importance: too high sample rates are not recommended and a too low one leads to aliasing. Therefore an optimal rate must be found according to the application. Furthermore, sampling can be used for down- and upsampling. That means the amount of data points, which represents a curve can be increased or decreased. An upsampling procedure can be advantageous for a smoother representation of the signal, whereby downsampling procedures are used to delete unnecessary

data, when a lower amount of points can depict the curve details in the requirements as well as the original signal.

Generally, it can be distinguished between three different filter types: a high pass-, a bandpass- and a low-pass filter. Band-pass filters let all frequencies within a defined band pass. Low-pass filters reject high frequency components above the cut-off frequency f_c. High-pass filters reject low frequency components from zero up to a defined number. The next chapter deals with a type of a high-pass filter: the DC-Blocking filter.

4.3 DC-Blocking filter

A DC-Blocking filter is a typical high-pass filter. The DC denotes that the DC-Blocking filter is used to remove constant frequency components of a signal. It works by combining differentiation and re-integration. Therefore, a filter coefficient between zero and one has to be determined to identify the amount of desired removal of signal components. A common value is a=0,99. It can be defined by trial and error but more persuasive is to determine a by its relation to the cut-off frequency (see chapter 4.2 and de Freitas (2007)).

Figure 4.16 shows an applied DC-Blocking filter on a signal with a=0,95. The original signal (black) consists of low frequency and high frequency components. As depicted the DC blocked signal (blue) is exempted from the low frequency component. (de Freitas 2007); (O'Brien et al. 2001)

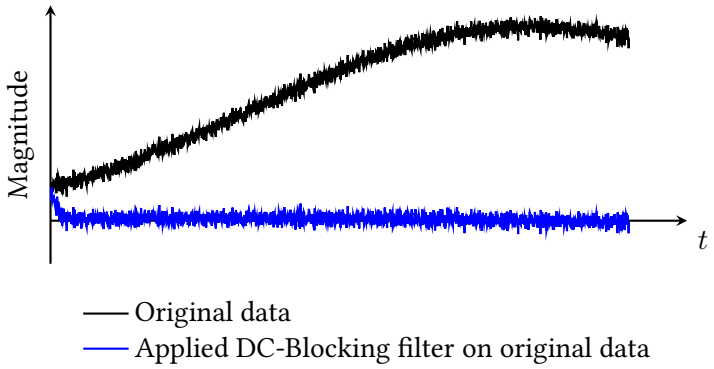

Figure 4.16: DC-Blocking filter with a=0,95 applied on data curve with high- and low-frequency components

In the next chapter, the prior discussed theory is used to developed the method of auralization and its application.

5 Transient Acoustic Simulations with Auralization

Transient simulations deal with dynamic problems in the time domain. This kind of simulation is advantageous for auralization tasks because auralization happens in the time domain and not in the frequency domain (see chapter 3). Whereupon, it is possible with inverse Fourier Transformation to convolute data from the frequency domain to the time domain (see chapter 4.1) but such an universe transformation is valid for small changes in the energy level only, for so-called stationary or quasi-stationary cases. Therefore, it is more convenient for auralization purposes, where normally high energy fluctuations occur, to simulate directly in the time domain to prevent the loss of relevant information through transformations.

In the following section a procedure is illustrated to auralize data from simulation.

5.1 Method to Auralize Transient Dynamic Simulation Data

The method developed and utilized in this work to make transient simulation data audible is illustrated in figure 5.1 and is based on the approach of O'Brien et al. (2001). The first column of figure 5.1, from discretization to node output, represents the transient dynamic simulation part.

In the first step a part has to be discretizised. In case of small deformation and linear problems the calculation time can be reduced by using modal-based methods instead of explicit or implicit dynamic simulation techniques. In this context the natural mode shapes, the so-called eigenmodes, are determined in a modal analysis to be included in a deformable rigid body simulation (abbr. DFB). DFB simulations are generally rigid body simulations with a superimposed linear modal response on the basis that every natural movement of a structure can be expressed as a sum of the response of each mode (see figure 5.2). In contrast the stiffness- and mass matrix of explicit or implicit methods are calculated based on a set of elements. Using a set of modes instead of a set of elements leads to a considerable reduction of degrees of freedom (abbr. DOF) and thereby to a high computational efficiency. Basically, modal methods

like modal superposition approximate the structural response by using a linear combination of pre-computed mode shapes.

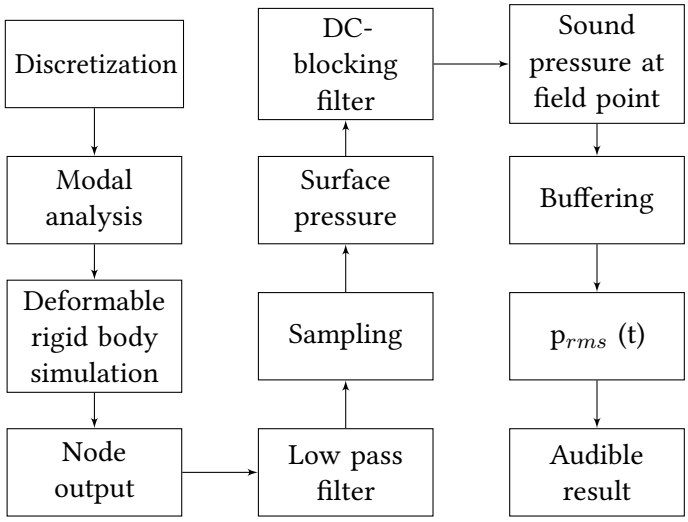

Figure 5.1: Auralization method for data from transient dynamic simulation

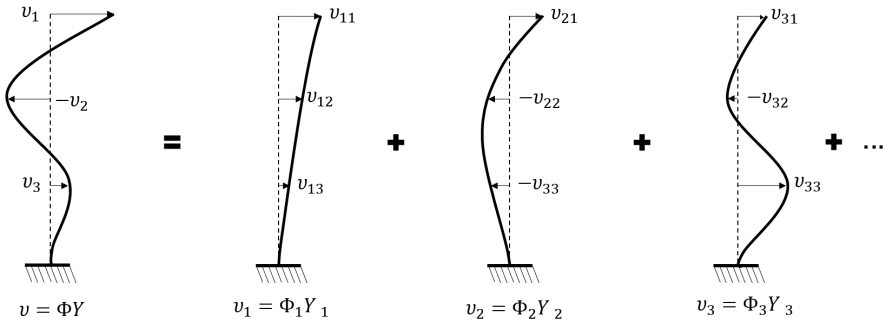

Figure 5.2: The principle of modal superposition: the result displacement consists of modal components (according to Kalny (2013))

Ideally, using the complete set of eigenmodes gives an exact response of the structure, i.e. the more modes are included, the more accurate are the results: figure 5.3 depicts a cutout of the force excitation of a cantilever motion[1] with different numbers of included eigenmodes compared to the implicit result and table 5.1 depicts the corresponding calculation

[1]Displacement measured at the excitation point.

time. (Blitzenbauer, Franz, Schulz & Mlekusch 2005); (Maker & Benson 2003); (Blitzenbauer, Franz & Schweizerhof 2005)

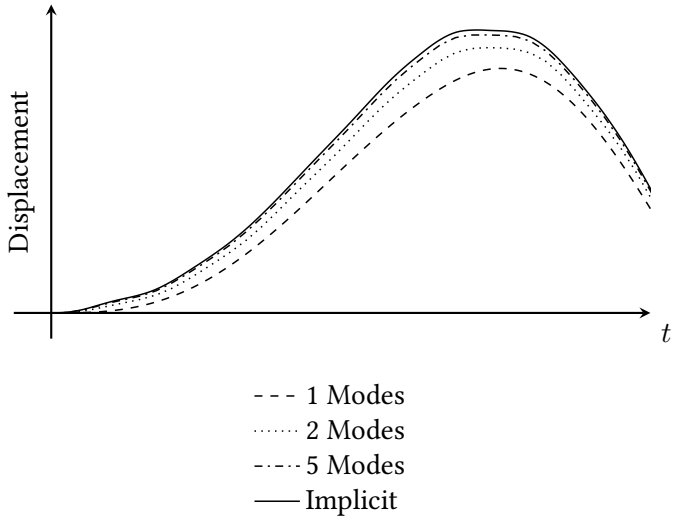

Figure 5.3: Influence of number of modes when using modal superposition principle compared to an implicit calculation

Table 5.1: Calculation time when using modal superposition

Included modes	Calculation time in min (16 CPU, 0,8 GB RAM)
1	3
2	4
5	5
Implicit	26

The deformable rigid body simulation is performed with a quadratic element mesh: figure 5.4 illustrates a discretized can for a crushing simulation with the used quadratic mesh shown on the left hand side. It is important that the discretization of the mesh represents the real design as well as desired in order to give adequate eigenmode results. Additionally, in order to auralize the motion later, a triangular mesh on the surface (center of figure 5.4) with no influence to the deformable rigid body simulation is adapted to the existing nodes. On the right hand side of figure 5.4 the combined quadratic mesh for the calculation of the eigenmodes and the triangular surface mesh for the auralization procedure is shown. In other words, the cylindrical part of the can is additionally meshed by triangular elements in order to output

its surface motion for the auralization. From experiences of life it is known that the largest deformation of a can happens in the cylindrical part because the material in the top and bottom are usually stiffer. Thus, the major part of the sound is emitted by the cylindrical part. For computational efficiency it is of key importance to choose the sound-emitting surfaces for the auralization wisely. At the end of the dynamic simulation part, an output file is created containing node coordinates, displacements and velocities of the surface mesh, which will be processed in the next steps. Basically, the dynamic simulation part can be done with most commercial FE-software packages.

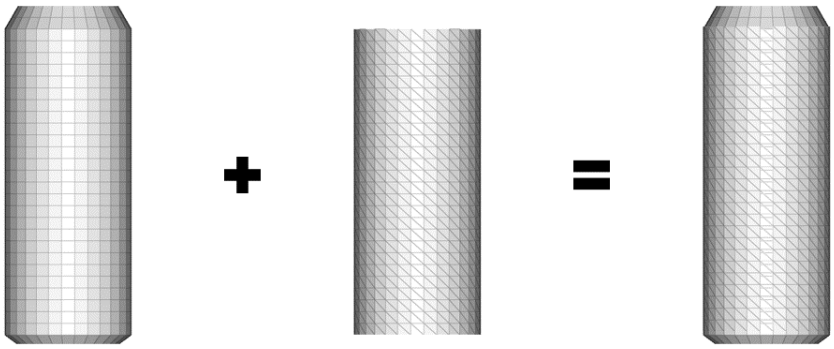

Figure 5.4: Discretization for dynamic simulation (left), surface mesh (center) and the final mesh (right)

The second column of figure 5.1 deals with data filtering. In order to get high quality results it is important to apply two filters. At first a sampling procedure needs to be used to generate an audio signal with a common sampling rate of 44100 Hz or 48000 Hz. As mentioned in chapter 4.2, to sample data it is important to apply a low pass filter initially to reduce the frequency band in order to sample the data up- or down with consideration of Nyquist-Shannon sampling theorem (see equation 4.8). With the sampled signal the pressure on the surface can be calculated. When assuming a plane wave[2] of the element sound radiation and neglecting viscous shear stresses, the acoustic pressure of the fluid adjacent to each element of the surface mesh, may be expressed by:

$$p = z\vec{v} \cdot \vec{n}, \tag{5.1}$$

where z is the specific or characteristic acoustic impedance (wave resistance), which can be written as z = ρ·c. In this context the air density ρ is ρ = 1.21 kg/m^3 at 20°C and 1 atm, and

[2] A plane wave is a wave with parallel and equally spaced (a wavelength apart) planes normal to propagation direction.

the wave speed is c = 343 m/s (Halliday et al. 2002). This leads to an acoustic impedance of z = 1.21 kg/m^3· 343 m/s = 415 Pa · s/m. Furthermore $\vec{n}$ is the unit vector normal to the surface element to detect the direction of distribution in order to calculate the velocity v in normal direction. The pressure p is calculated for each time step and each surface element. It expresses the pressure fluctuation adjacent to the surface in normal direction.

Afterwards the DC-Blocking filter (chapter 4.3) is applied to remove constant components of the signal: e.g., an object moving through an environment with a constant velocity, a constant pressure occurs in front of it, which results in an offset of the pressure amplitude. A DC-Blocking filter removes such undesired components. Furthermore, the application of the DC-Blocking can be avoided by the usage of relative coordinates, the so-called local coordinates, where pressure fluctuations only and therefore no constant values appear: by using local coordinates in the latter example the constant velocity has no influence on the pressure change because the coordinate system is moving with the velocity of the object.

As mentioned, the application of filters can improve the quality of the result. In this context it is important to analyse the system initially and to find a suitable sampling rate for the certain problem. Furthermore, within this work it becomes evident that with increasing model size, the sampling rate needs to be reduced in order to decrease the simulation time and to avoid huge output files.

In the next step, the sound pressure is calculated at a given point in the field. Therefore the pressure of all elements for each time step are summed up according to Huygens' Principle (see chapter 2.2). Thus, the wavelets of the point sources of the elements are treated as initial points for a new wave front, which is represented by the envelope of all wavelets. In order to calculate the wave propagation of this envelope to an arbitrary point, the equivalent radiated power density[3] of one element may be considered:[4]

$$ERP_\rho = \frac{1}{2}\rho c \cdot v_n(r)^2, \tag{5.2}$$

where ρ defines the fluid density, c the sound velocity and $v_n(r)$ the normal velocity on the surface with a distance of r from the source. The equivalent radiated power density ERP_ρ describes the acoustic intensity $ERP_\rho = I$ of any point with the distance of r to the source for

[3] Generally, ERP ρ is a complex quantity and depends on the distance (real part) r and the frequency (imaginary part) f. However, the auralization is happening in the time domain depending on the distance r and therefore the frequency (imaginary part) is not relevant in this work and therefore not further mentioned.

[4] All values in equations denote maximum values to simplify the reading. Effective values are written with indexed rms (root mean square) e.g. p_{rms}. Note: $p_{rms} = p_{max}/\sqrt{2}$

far fields and high-frequencies starting from approximately 500 Hz. Introducing the impedance z=ρ·c=p/v equation 5.2 can be rewritten as:

$$ERP_\rho = I = \frac{1}{2} z v_n(r)^2 = \frac{z p(r)^2}{2z^2} = \frac{p(r)^2}{2z} = \frac{p_{rms}(r)^2}{z}, \tag{5.3}$$

where p denotes pressure and v velocity. Furthermore it is useful to take the absolute equivalent radiated power $ERP_{absolute}$ of one surface element into account:

$$ERP_{absolute} = \frac{1}{2}\rho c \int_A v_n(r)^2 \, dA. \tag{5.4}$$

The $\text{ERP}_{absolute}$ relates the acoustic power W_s of the source (surface element) as follows:

$$W_s = ERP_{absolute} = \int_A I_s \, dA = I_s A, \tag{5.5}$$

where I_s is the sound intensity of the source and A the area of the surface element. Combining equation 5.3 and 5.5 allows to express the power of the sound source as follows:

$$W_s = \frac{p_s^2}{2z} A. \tag{5.6}$$

Furthermore, the power of the field point W_{fp} may be expressed as:

$$W_{fp} = \oint_A I_{fp} \, dA = I_{fp} 4\pi r^2, \tag{5.7}$$

where W_{fp} is the power of the spherical wave field around the field point and r the distance between sender and receiver. This relation is commonly expressed as:

$$I = \frac{W}{4\pi r^2}, \tag{5.8}$$

in the so-called inverse-square law: the intensity is inverse proportional to constant/r^2, because the power W is constant. Figure 5.5 illustrates the inverse-square law with a section of a spherical wave. The sound power constantly propagates from the source S with an increasing area. Thus, the amount of power per unit area (intensity) is decreasing.

Furthermore, the power equation of the field point (equation 5.7) combined with the equivalent radiated power density (equation 5.3) leads to the following expression:

$$W_{fp} = \frac{p_{fp}^2}{2z} 4\pi r^2. \tag{5.9}$$

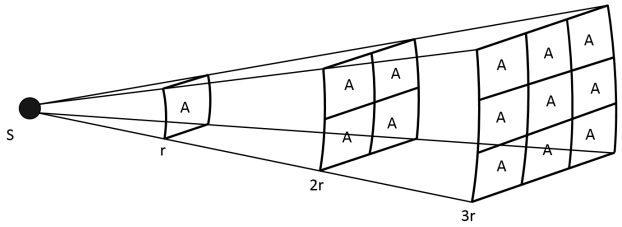

Figure 5.5: The inverse-square law (according to UdK Berlin (1998))

In this context, it is practical to assume a free sound propagation (no damping and no reflection) in order to achieve a power balance between the surface element and the field point with $W_s = W_{fp}$ (equation 5.6 and 5.9):

$$p_{rms,fp} = \frac{p_{rms,s}}{2\sqrt{\pi}r} \cdot \sqrt{A}. \tag{5.10}$$

Furthermore, it is of key importance to consider the spatial arrangement of a surface element and the field point in order to consider the directional pattern. This defines the amount of the acoustic wave, which is emitted from one surface element to the field point. Figure 5.6 shows exemplary different directional patterns in polar coordinates, where the black vertical line represents one element oscillating in horizontal direction with the velocity v.

Thereby, depending on the specific case, different directional patterns can occur. The continuous black curve depicts the radiation characteristics of an acoustic dipole, whose main lobe can be described as $\pm cos(\varphi)$ function. A piston radiator[5] propagates sound within a small lobe (dotted curve) and a speaker at 63 Hz (dashed curve) generates a wider and more diffus sound propagation than a dipole. Furthermore, the directional patterns for speakers change at different frequencies. Generally can be said: the higher the frequency, the smaller the lobe and thus, the higher the amount of lobes. Subsequently, the sound propagation strongly dependents on the system and the frequency band of the signal. According to O'Brien et al. (2001) and Kinsler et al. (2000) $cos(\varphi)$ is a useful approximation for the main lobe of the frequency-dependent function for flat elements. Basically, the $cos(\varphi)$ function means that the pressure fluctuation of each element is weighted concerning the direction of propagation: the closer the angle of the field point to 180° or 0°, the larger the amount of transmitted pressure. In other words, the larger the angle between the surface normal and the field point, the smaller

[5] A piston radiator emits small wavelength waves compared to its size.

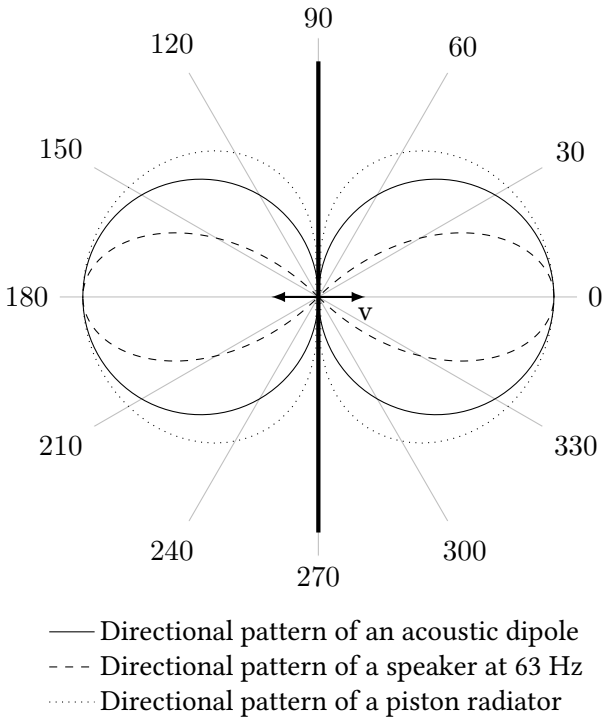

Figure 5.6: Sound radiation characteristics (according to Will (2017))

the amount of depending pressure. In order to consider the sound directional characteristics a $cos(\varphi)$ in normal direction to the surface elements is added to equation 5.10:

$$p_{rms,fp} = \frac{p_{rms,s}}{2\sqrt{\pi}r} \cdot \sqrt{A} \cdot cos(\varphi). \tag{5.11}$$

However, the equation above is a rough approximation to calculate the pressure from a source to a field point but during this work this equation showed comprehensible results and is generally very promising regarding computational time compared to more detailed equations e.g. Kirchhoff's integral theorem (see equation 2.4). Furthermore from O'Brien et al. 2001 it is known, that similar approximation functions from image rendering are already used for auralization purposes. (John H. Lienhard IV and John H. Lienhard V 2008); (Wendt 2016); (Wiechmann & Hiller 2011)

With equation 5.11, the pressure in each time step at the field points can be calculated. In this context it is important to consider the propagation delay in order to create a realistic sound

because naturally, waves from surface elements closer to the field point reach the field points faster than the ones from more distant. This behaviour can be considered by:

$$delay = \frac{r_{s-fp}}{c}, \tag{5.12}$$

where r_{s-fp} is the distance between the surface element and field point and c the sound velocity. Therefore, the audio samples will be stored in an one-dimensional buffer according to their occurring time plus delay. In this context it is unlikely that a sample meets an exact time point of the sampling rate. Moreover the samples are mostly in between two sampling points and the value of the sample has to be added somehow to the buffer. Figure 5.7 illustrates a sample (black dot) with the calculated time t=3.4 and a certain amplitude. The next sampling points are 3 and 4. Thereby the value of the sample has to be added to a buffer, either into buffer 3 or 4. It seems convenient to round the calculated time of the sample to the nearest entry in the buffer. In this case the value of the sample would go into buffer 3 and would be added up to the value of c.

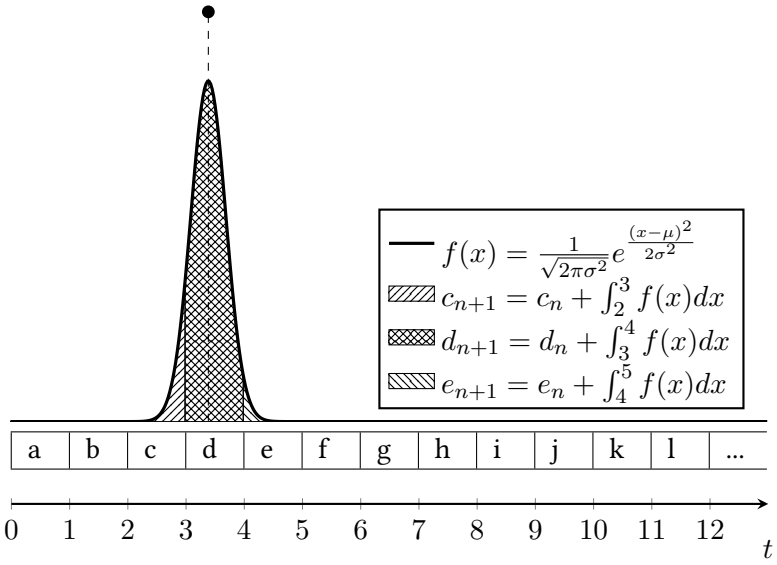

Figure 5.7: Buffering of a sample

However, in case t would be t=3.5 the value of the sample would be added up to the value of d. Thus, a small variance of time influences the buffer number enormously. In other words, especially, the high probability that more samples are accidentally closer to a certain sampling point results in local maxima and therefore in artifacts, unpleasant buzzing sounds and a kind of saw-tooth wave in the generated sound (see figure 5.8). Therefore, it is practical to use a

two-sample-wide Gaussian distribution f(x) to split the value of the sample into three parts for three sampling points of the buffer (see figure 5.8). The area under a Gaussian distribution is always 1. That means that the value of the sample can easily be multiplied by the integral from two following samples. The hatched area under the Gaussian on the left between 2 and 3 represents the portion of the value of the sample which will be added to c, the integral from 3 to 4 to d and the remaining part of the value to e. In this context figure, 5.8 depicts the difference between distributing the samples by Gaussian and rounding the samples to the closest sampling point. The curve of an applied rounding function shows the mentioned saw-tooth components with high amplitudes, whereas the curve with Gaussian distribution indicates a smooth characteristic.

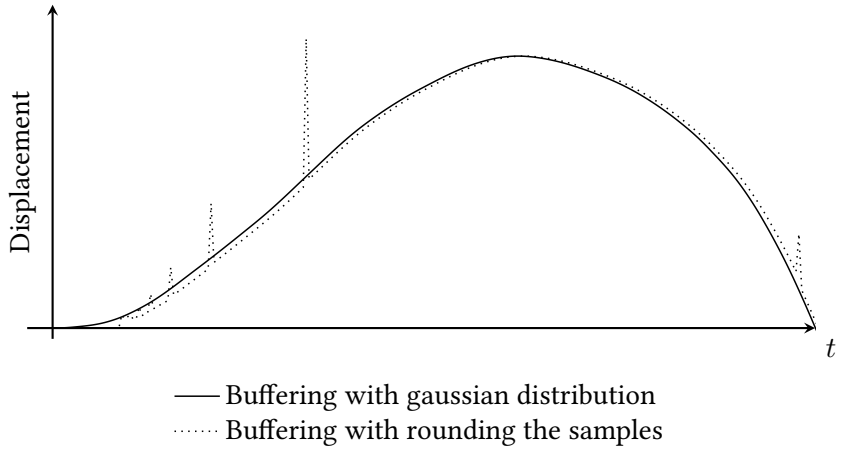

Figure 5.8: Distribution of samples for buffering

After buffering, the effective sound pressure is determined for each time step according to its delay. In the last step the pressure will be transformed into an audible result. A common audio format for this purpose is the wave format. Normally, the amplitude of wave files is within a range of -1 to 1. Therefore, it is necessary to normalize the audio signal to avoid clipping[6] in order to transform it into a wave file. For stereo sound the pressure of two field points can be calculated and added for each ear as left and right channel together.

The method described in this section has been applied in several examples as described the following sections.

[6] Clipping describes the cut off in the time domain above a certain amplitude, which leads to distortions of the signal.

5.2 Cantilever

A classical cantilever is a beam or plate excited by a force on one side and restrained at the opposite side in all degrees of freedom. Figure 5.9 depicts schematically the cantilever used in this work.

Figure 5.9: Schematic model of a cantilever

According to the auralization method described in the previous chapter (see figure 5.1), the first step is to discretize the cantilever for the simulation. Figure 5.10 illustrates the model of the cantilever: the cantilever is restrained at one end in all DOF and on the other end forces are applied in three nodes (see left hand side). The forces are applied for a very short time in the beginning of the simulation to excite the cantilever into a swinging motion with the objective to make this oscillation audible. The right hand side of figure 5.10 shows the exploded view of the cantilever with the quadratic structure mesh at the bottom and the triangular surface mesh at the top.

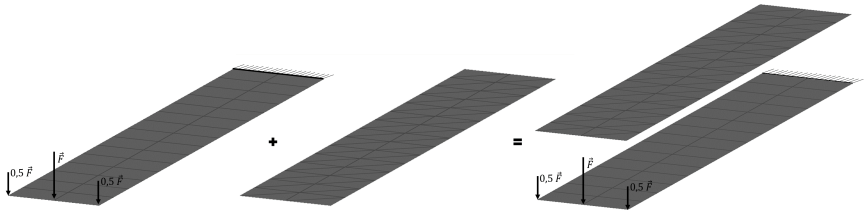

Figure 5.10: Discretized model of cantilever for transient simulation (left), for auralization (center) and its exploded view (right)

In order to improve the method and develop scripts for this procedure a computationally cheap and simplified model of a cantilever is used, which consists of 48 nodes, 30 quadratic shell elements for the structure mesh and therefore of 60 triangles for the surface mesh (see table 5.2).

In the following next step, the eigenmodes have to be determined to include them in a deformable rigid body simulation. Therefore, it is of key importance to analyse the influence of the modes initially in order to detect the lowest amount of modes, which can represent

Table 5.2: Mesh properties of cantilever model

	Structure	Surface
Nodes	48	48
Elements	30	60

the structural motion. Figure 5.11 shows the first five eigenmodes and its original position (dashed).

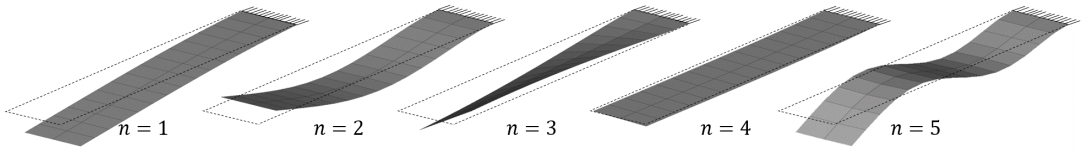

Figure 5.11: First five eigenmodes of the cantilever

It is reasonable to assume, that a uniformly applied force at one end of the cantilever leads primarily to a first mode motion (n=1). Therefore, to see the influence of more excited modes, the values of the outer forces in the used model are half as high as the middle force (see figure 5.10). Figure 5.12 illustrates a cutout of the displacement[7] of different numbers of included modes compared to the implicit calculation. It can be observed, that after the first amplitude, which represents the displacement of the force excitation, all curves quickly overlay. This means, that after the excitation the influence of upper modes are negligible because the cantilever moves in a pure first mode. Therefore, the different values of the forces affect the movements directly in the excitation time only because the stiff response of the small amount of elements eliminate immediately any other kinds of mode shapes in the free motion.

However, five modes are included in the deformable rigid body simulation of the cantilever due to the high accuracy during the excitation time with a very limited computational effort. During the simulation the displacement and velocity is recorded for each node of the surface mesh in each time step. Then the sampling procedure can be applied. Afterwards, the surface pressure of each element is calculated. The DC-Blocking filter does not have to be applied in this model because constant motion does not occur and therefore constant pressure is not generated.

In the next step, the pressure change at a selected field point can be made audible. Figure 5.13 depicts exemplary the creation of a stereo sound. Therefore the pressure fluctuations at two field points for both ears have to be calculated: a line is used from the center point of

[7] The displacement is measured at the middle force node.

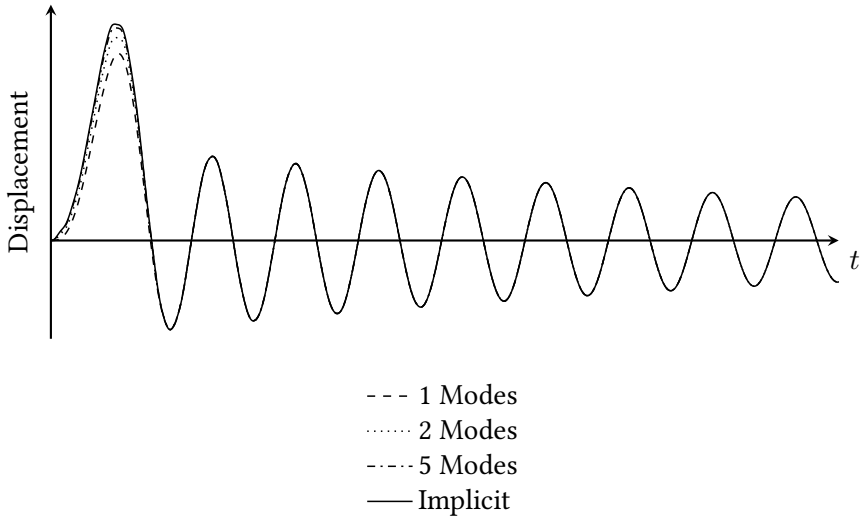

Figure 5.12: Influence of included modes on cantilever motion

the human head (black dot) towards the cantilever in order to create two field points (small black dots) for both ears perpendicular from the center point with a approximated distance of $\pm$ 10 cm. The calculated pressure time series of both ear points are joined together as left- and right channel. This stereo sound of the cantilever motion can be found in the attachment 'Cantilever.m4a'.

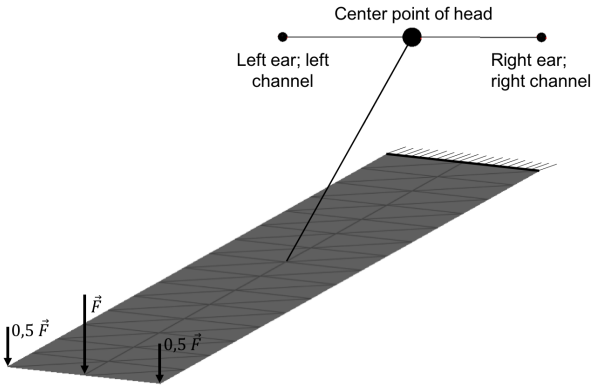

Figure 5.13: How to create a stereo sound?

Furthermore, in a next step, this example is used to analyse the influence of the element size of the surface mesh on the audible result. As mentioned, the surface mesh is used for the

auralization procedure only and does not influence the FE simulation: basically, it is used to define independently the sound emitting surfaces from the structure mesh in order to track the motion of its nodes. Figure 5.14 shows four different surface meshes of the cantilever: on the top, the mesh of the carried out cantilever auralization is depicted (see figure 5.10), which represents a fine mesh and is used as reference for the two rougher meshes below and the only acoustic meshed tip of the cantilever at the bottom.

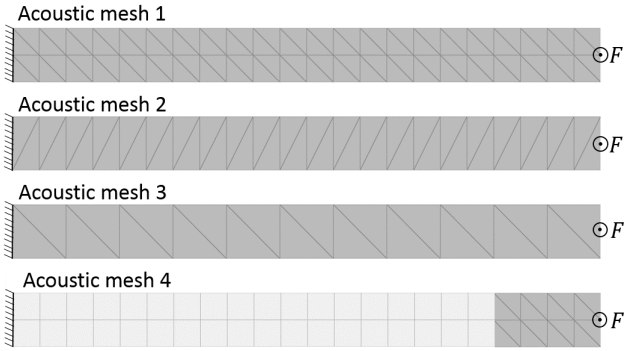

Figure 5.14: Analyse of four different acoustic meshes of the cantilever (mesh sensitivity)

Figure 5.15 shows the generated sound with the different mesh sizes in the time domain: it can be noticed, that the amplitude decreases with a rougher mesh. This happens because this auralization approach sums the surface pressure of all elements, which means the more elements are used, the higher the sound pressure: this method is not developed to predict the amplitude precisely but moreover to determine the time dependent variation of the sound pressure signal. In other words, this method should calculate the characteristics of the sound with an approximated amplitude: at the end of the auralization procedure a wave file is generated, which basically consists of normalized values between -1 and 1. Therefore, the amplitude of this sound can be adjusted manually by the playback sound level of the playing device (e.g. computer).

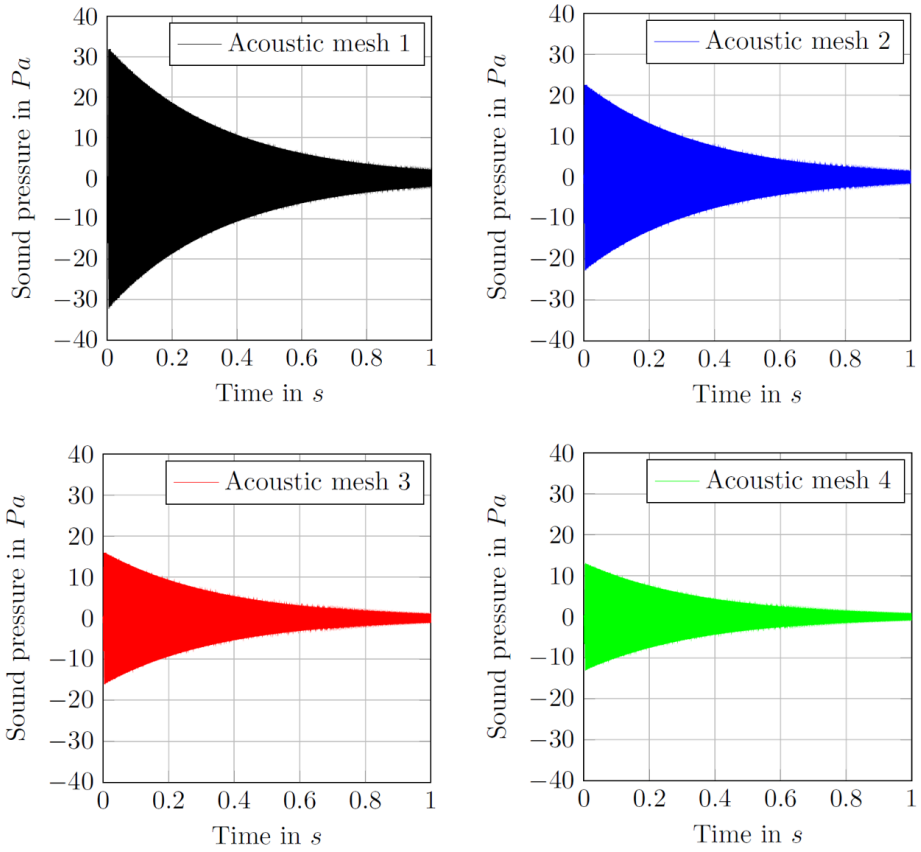

Figure 5.15: Influence of the mesh size on the time domain signal

In order to evaluate the sound characteristics more in detail, figure 5.16 represents the spectra of the time domain signals in a range from 0 Hz to 1000 Hz. The peaks at 440 Hz indicates a resonance frequency of the cantilever. Furthermore, all curves have slightly different amplitudes due to varying amplitudes in the time domain. However, the curves show very similar progresses and even the curve 4 with the meshed tip only represents a similar spectrum. This similarities illustrate, that the mesh size is not really relevant for the sound characteristics apart from the amplitudes, but this method is, as mentioned, not developed to predict the amplitude in detail. Therefore, it is convenient regarding the calculation time of the auralization procedure to concentrate more on the sound characteristics and use rougher meshes. Furthermore, according to the result of mesh 4 it is possible to discretize the most relevant sound emitting areas only in order to get almost as accurate results as with a complete surface mesh. However, for

more complex parts it can be sophisticated to determine the most relevant sound emitting areas.

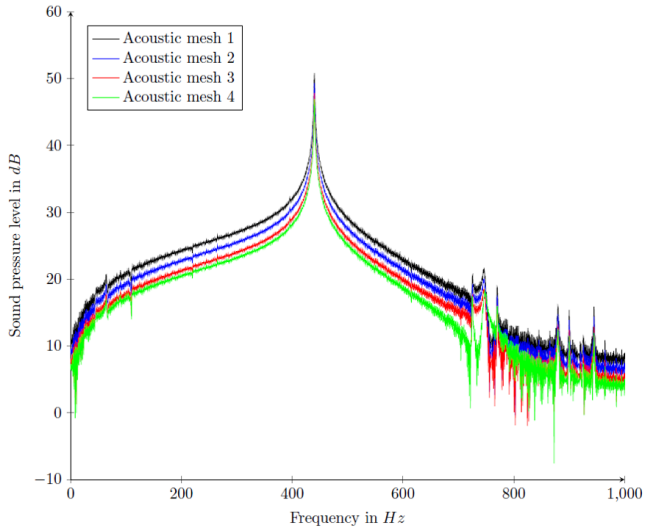

Figure 5.16: Influence of the mesh size on the frequency domain signal

Scripts were developed within the cantilever example in 'HyperMath' and 'Scilab' to automatize the application of the auralization method: the 'HyperMath' script automatically processes the simulation results from the node output to the buffered pressure time series at the field point (see figure 5.1). The 'scilab' script converts the pressure into a sound file. In this context the following table shows the computational effort of the simulation and the auralization process:

Table 5.3: Computation time of cantilever model

	Simulation (16 CPU, 0,8 GB RAM)	Auralization (2 CPU, 12 GB RAM)
Time in min	5	1

The applied auralization method on a cantilever motion shows promising results. However, adequate experimental data for comparison is not available and therefore it can not be evaluated how close the results are to reality. Nevertheless, a swinging metal can be imagined from the sound, but, as mentioned, a substantial statement can not be made. For a more convincing verification, a second example known from life and easy to replicate is used: a sound of a ball dropping on a surface.

5.3 Ball Drop

In this chapter a simulation of a dropping ball on a surface has been made audible according to the auralization method in figure 5.1. Figure 5.17 shows the simulation model, which consists basically of a plane and a ball. A gravitational field is applied with g=9,81 m/s^2.

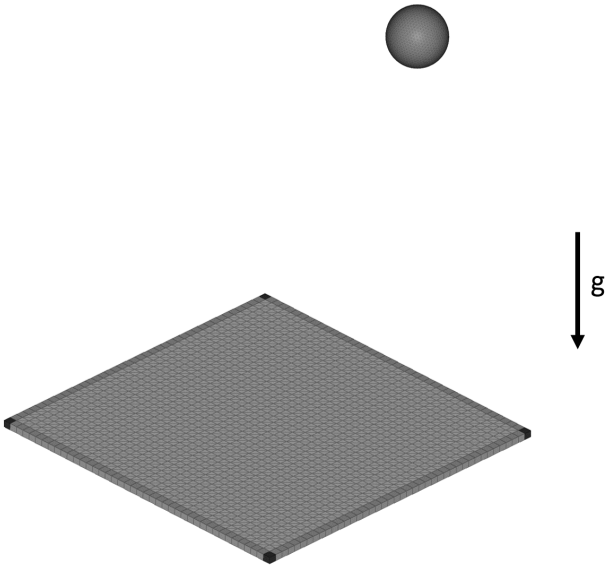

Figure 5.17: Simulation model of ball drop example

The ball is initialized with a horizontal velocity in order to generate a line of drops on different locations on the plane. Furthermore, the plane is fixed in all degrees of freedom in all corners illustrated with black quadratic elements. This simple case is promising for the verification of the auralization method because it is possible to assess if the generated sound is realistic. Furthermore, it is a very limited effort to replicate the chosen case in an experiment.

Figure 5.18 illustrates the mesh of the plane in an exploded view: the structure mesh (at the bottom) consists of quadratic elements and the surface mesh is depicted in triangles. Moreover, the ball consists of tetrahedron elements, which is visualized in figure 5.19. Table 5.4 shows more detailed information about the parts and its elements and nodes.

Table 5.4: Mesh properties of the ball drop model

	Structure of plane	Surface of plane	Ball
Nodes	3690	1681	3166
Elements	1760	3200	14159

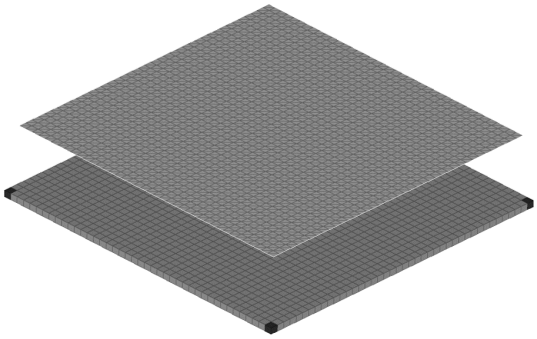

Figure 5.18: Exploded view of the structure and the surface mesh

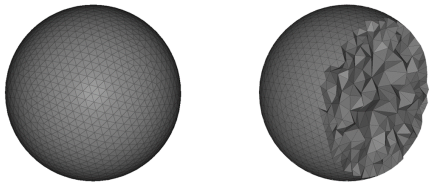

Figure 5.19: Tetrahedral mesh of the ball

Furthermore, the plane is designed as deformable rigid body with 20 superimposed modes, which can represent frequencies up to approximately 7800 Hz. The ball is simulated as rigid body because its elastic deformations are very small compared to the elastic deformation of the plane. Thus, not only the deformation of the ball is neglected but also its emitting sound. This simplifies the model and decreases the simulation time without loosing significant information. The sampling rate for the node output is 20000 Hz to cover frequencies regarding Shannon-Nyquist sampling theorem up to 10000 Hz, which is sufficient for the occurring frequencies. Furthermore, within this example the low-pass filter and the sampling is used to up sample the signal to 22500 Hz in order to investigate the up sampling capabilities of the script. In the next steps, the surface pressure is calculated. The DC-Blocking filter does not need to be applied because of no occurrence of a constant pressure in the signal (no constant motion). Then the pressure fluctuations are determined at a specific field point and buffered afterwards. The generated sound is located in the attachment 'BallDrop.mp4'. Table 5.5 shows the calculation time of this model:

Table 5.5: Computation time of ball drop model

	Simulation (16 CPU, 0,8 GB RAM)	Auralization (2 CPU, 12 GB RAM)
Time in h	6	18

The generated audio signal and especially the ball rolling on the surface sounds very realistic. Nevertheless, it can not be quantified how close the results are to reality and therefore, a system with a specific characteristic and a measurable sound is used in the next example in order to compare the auralized sound with experimental data.

5.4 Vibraphone Bar

A vibraphone a musical percussion instrument with a playing range of three octaves.

Figure 5.20: The vibraphone (Lone Star Percussions 2016)

The main elements of a vibraphone, as illustrated in figure 5.20, are a supporting stand, different metal (vibraphone-) bars with resonators and a damper. The damper can be excited with a paddle. Once the damper is activated, felt pads are pressed against the bars which can damp their vibration. The bars are excited by mallets. Each of the bars has another fundamental frequency according to its length. Furthermore, this vibraphone has tube resonators, which are located vertically under each bar in order to amplify the sound of the specific fundamental frequency of the bar above. The resonators have an open end towards the bar and a closed end

on the other side and are therefore often referred to as one-end-open tubes. A vibrating bar emits a relevant amount of pressure waves into the one-end-open tube. At the closed end the waves get reflected and move back towards the opening. Thereby, each resonator is designed to amplify the fundamental frequency of the bar above. This is realized by different lengths of the resonators in order to generate so-called standing waves inside of the tubes (see figure 5.21). The phenomenon of standing waves can be described by two waves moving with the same frequency and amplitude in opposite directions into each other, which overlay and form one amplified wave. This overlaid wave has so-called nodes or stationary points, where the amplitude is always 0 and all the other points of the wave have constant amplitudes. In the case of the vibraphone: the wave from the bar emits into the resonator and is reflected on the lower side, whereby the incoming and the reflected wave overlay.

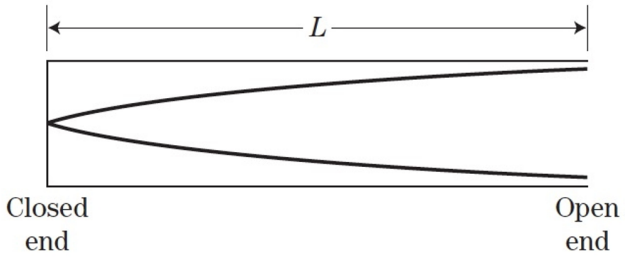

Figure 5.21: A standing wave of the fundamental frequency in an one-end-open tube (Russel 2012)

Generally, the resonator length L and the wave length λ may be expressed for an one-end-open tube by:

$$L = (2n + 1)\frac{\lambda}{4}, \tag{5.13}$$

where n describes the amplified mode number with n = 0,1,2,3,... . In the case of the vibraphone the fundamental frequency n=0 should be amplified, which leads to the following expression:

$$L = \frac{\lambda}{4}. \tag{5.14}$$

This means, that the length of the resonator should be a quarter of the wave length to amplify the fundamental frequency: figure 5.21 depicts horizontally a half section view of such a standing wave of the fundamental frequency in the resonator. In order to amplify the different fundamental frequencies of the bars, the resonator length varies depending on the

wave length of the fundamental frequency of the bar (see figure 5.20). (Baader 2002); (Wendt 2016)

Within this work only one bar with a resonator of the vibraphone is used. Figure 5.22 shows the used vibraphone bar and its resonator. It is designed to generate the tone a_2 with a fundamental frequency of 880 Hz. In order to amplify the fundamental frequency, the resonator of this type of vibraphone has a rectangular cross section. This does not change the properties significantly compared to the mentioned circular cross section but it is just more practical for single vibraphone bars because it does not need any additional attachments to stay upright.

Figure 5.22: The vibraphone bar with resonator analysed in this work

Figure 5.23 shows the resonator and its three openings. On the top of the resonator are two pins to fix the position of the bar relative to the resonator. Furthermore, the bar is positioned on four rubber supporting points.

Figure 5.23: The resonator without the vibraphone bar

In the following sentences the properties of the used vibraphone are evaluated. Figure 5.24 shows the dimensions: total height h_{total}=8,1 cm, total width w_{total} = 16,9 cm and bar thickness t_{bar}=0,5 cm. Furthermore, the height of the resonator is $h_{resonator}$ = 7,0 cm and its wall thickness is t_{wall}=0,2 cm.

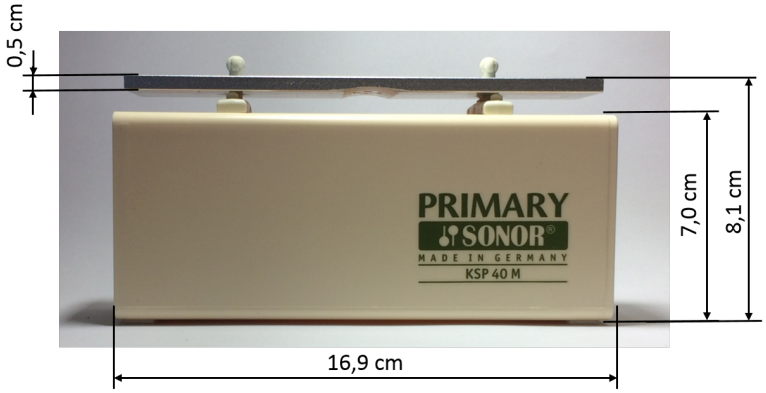

Figure 5.24: The dimensions of the vibraphone (side view)

The standing wave is oriented in vertical direction, that means, according to equation 5.13, that the height of the resonator should be 4 times smaller than the wave length of the fundamental frequency. The wave length λ may be calculated by using its relation to sound velocity c and the frequency f:

$$\lambda = \frac{c}{f}. \tag{5.15}$$

The sound velocity is roughly c = 343 m/s at 1 atm and 20°C (Halliday et al. 2002). That means for the fundamental frequency of f = 880 Hz, that $\lambda_{880\ Hz}$ = c/f = (343 m/s) / (880 Hz) = 0,38978 m = 38,978 cm. According to equation 5.13 the amplifying mode number can be calculated with:

$$n = 2\frac{h_{resonator} - 2t_{wall}}{\lambda} - \frac{1}{2} = 2\frac{(0,07 - 2 \cdot 0,002)m}{0,38978m} - \frac{1}{2} = -0,1613 \tag{5.16}$$

As expected, the value of n is close to zero. Thus, the fundamental frequency of the vibraphone will be amplified.

For further information: the value of n is not exactly zero because the real height of the resonator does not completely match the theoretical height for amplifying the fundamental

frequency. The theoretical height of the resonator is $h_{theoretical,resonator}$ = 0,25 $\cdot\lambda_{880Hz}$ = 0,25 · 0,38978 m = 0,0975 m = 9,475 cm. The difference between the real height and theoretical height for amplifying the fundamental frequency of the vibraphone is $h_{resonator}$ - $2t_{wall}$ - $h_{theoretical,resonator}$ = 7,00 cm - 0,40 cm - 9,475 cm = -2,875 cm. This length difference occurs because the theoretical height calculation does not consider effects of the pressure wave when passing the openings. Therefore the real resonator height differs from the calculated value. The determination of the real height of the resonator in combination with the appropiate distance between the top of the resonator and the bottom of the vibraphone bar can be determined by experiments or with further calculations with the so-called end-correction. For further information about the end-correction is refered to Chen-Yih (1996) and Liljencrants (2006).

In the next chapter the acoustics of the vibraphone are experimentally investigated.

5.4.1 Experiment

The vibraphone experiment is performed in a semi-anechoic acoustic chamber. The left hand side of figure 5.25 shows the vibraphone bar with its resonator in the chamber. A microphone is placed 30 cm above the bar in order to measure the pressure change over time.

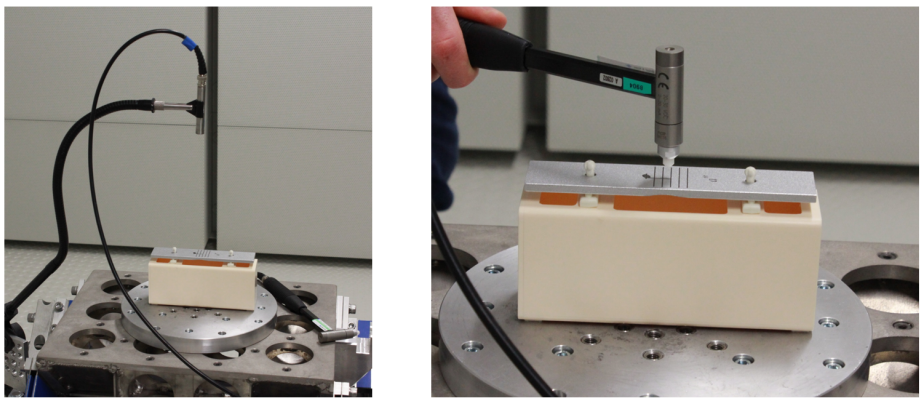

Figure 5.25: The vibraphone in the acoustic lab (left) and its on-center excitation (right)

The vibraphone bar is excited by an impact hammer in the middle (on-center) of the bar (see right hand side of figure 5.25). The impact hammer is used to measure the excitation force over time. This excitation characteristic is especially important for the simulation input to generate an excitation as close to the experimental value as possible. Figure 5.26 depicts the measured

excitation forces of three experiments. It can be seen that e.g experiment 3 has more than one peak. That means, that the excitation of the bar by the hammer happens more than one time. This occurs i.a. due to the planar shape of the impact hammer tip, because this tip touches naturally more than one point (planar contact). An optimal shape, as usually used in music, would be a spherical tip in order to create a point contact only. As depicted, the first force peak of each curve varies due to the manual excitation in a range from approximately 10 N to 30 N. However, the exact values are not important because in this work the impact hammer is used to identify the characteristics only. Therefore, the first peaks were evaluated to average the excitation force and the depending time, respectively: the following characteristic are used within the simulations: $F_{excitation}$=18,0 N with a duration time of $t_{excitation}$=0,5 ms.

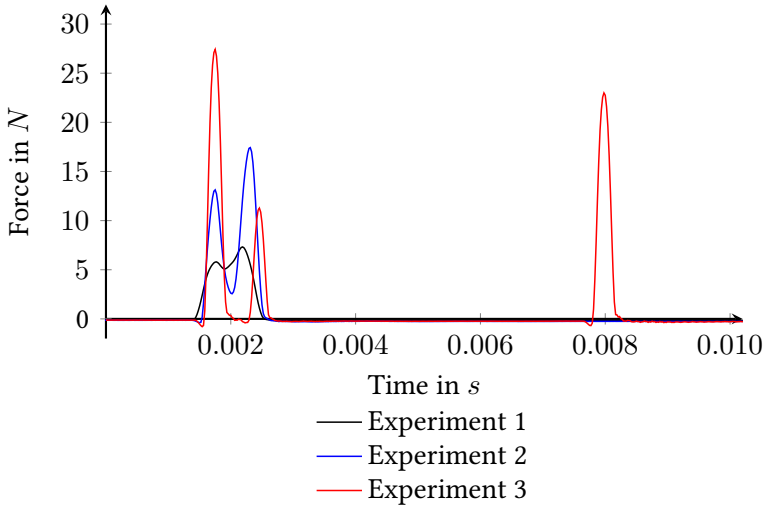

Figure 5.26: The measured force of the impact hammer

Figure 5.27 represents the results of the first 10 s of the experiment: the left hand side depicts the normalized sound pressure in the time domain, which shows from the normalized pressure of 1, -1 to almost 0 at the end of the curve a clear damping characteristic. Furthermore, after the high excitation peak in the beginning, the time domain signal decreases and then increases again. This effect occurs supposedly due to the mentioned tip of the impact hammer: after the excitation, the hammer tip remains naturally for a short time on the bar with its full circular area because the user can not remove the hammer immediately. During this time, the bar can not move freely because it is pressed more into the constraints (more damping), which decreases the amplitude of motion. After removing the hammer, the bar is more released from the constraints (less damping) and the natural movement of the bar takes place, which

results in a small amplitude increasing. For a simplified comparison of the experiment and the simulations this effect is neglected and only the 'released' motion is compared.

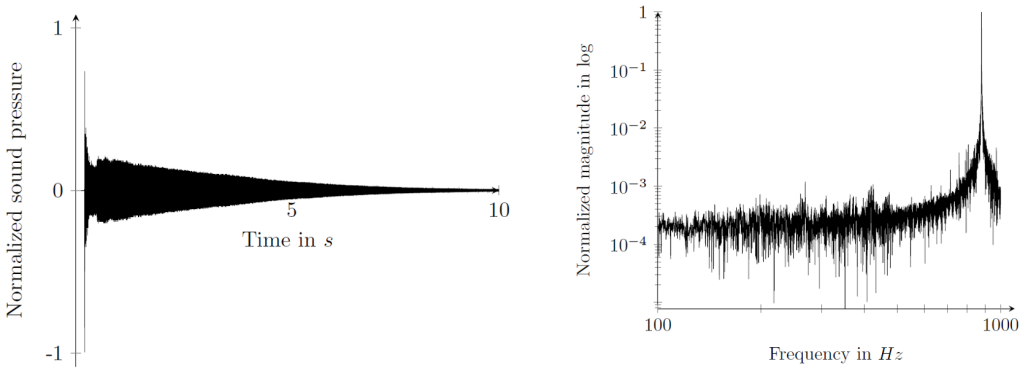

Figure 5.27: The measured signal of the vibraphone in the time domain (left) and in the frequency domain (right)

On the right hand side, figure 5.27 shows its frequency spectrum obtained by FFT from the time domain signal. The spectrum shows a range from 100 Hz to 1000 Hz only because the validation of the simulations and the experiment is going to happen in this range in order to especially evaluate the depiction of the fundamental frequency[8]. According to the discussed vibraphone theory, this curve shows the very pure fundamental frequency of 880 Hz because the specific constraints of the bar allow mainly the motion of the fundamental mode, which leads to a possible negligence of all the upper modes: In addition, figure 5.28 depicts a waterfall plot of an on-center excitation (left hand side) and an off-center excitation (right hand side): it illustrates according to the theory of the vibraphone, that in case of the on-center excitation, a very pure fundamental frequency is excited and damped out over time. The off-center excitation shows along to the fundamental frequency more frequency components in the beginning, which are according to its design soon damped out and a pure fundamental frequency is remaining.

In the next step another important information, the damping, is extracted from the experiment to provide the value for the simulation set up. Basically, damping describes the energy dissipation properties of a system under stress. Moreover damping characterises the decay of

[8]This spectrum is used in chapter 5.4.4 to validate the realism of the simulation method.

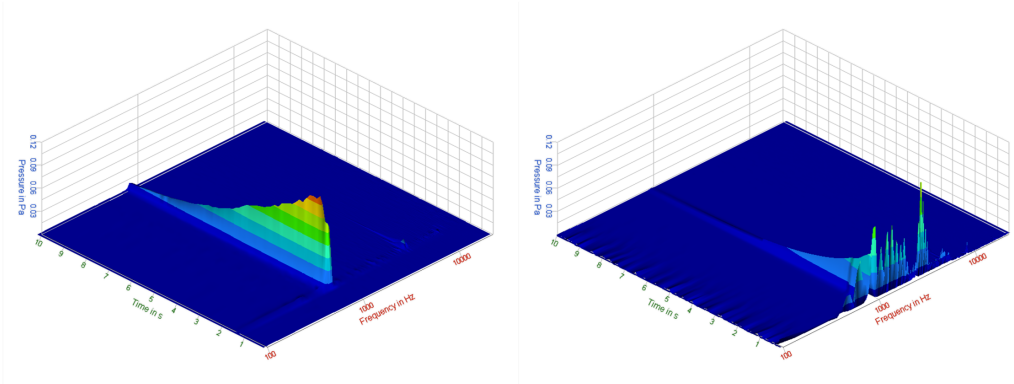

Figure 5.28: Waterfall plot of an on- and off-center excitation

oscillations after an excitation. In this context, it is useful to consider the equation of motion of a 1 DOF system, which may be expressed by:

$$m\ddot{x} + c_d\dot{x} + k_s x = 0, \tag{5.17}$$

where x represents the position and its derivatives (velocity, acceleration), m is the mass of the system, c_d the damping and k_s the spring constant. The damping is commonly expressed as the damping ratio ζ:

$$\zeta = \frac{c_d}{c_{critical}}, \tag{5.18}$$

where $c_{critical}$ is the critical damping of the system:

$$c_{critical} = 2m\sqrt{km}. \tag{5.19}$$

The $c_{critical}$ describes the quickest approach of the movement to zero amplitude. In other words, the critical damping of the vibraphone means, when the bar gets excited it moves from the initial position to the maximum displacement. After returning to the initial position the motion stops. This means, that the motion is already completely damped out after a half oscillation. This behaviour would be visible at a damping ratio of $\zeta = 1$ (critical damping). A system is overdamped when the approach to zero is slower ($\zeta > 1$). An underdamped system ($\zeta < 1$) is characterised by a damped oscillating motion. $\zeta = 0$ describes an continuously oscillating system with the same amplitude and without any damping. Figure 5.29 presents the different damping cases over time.

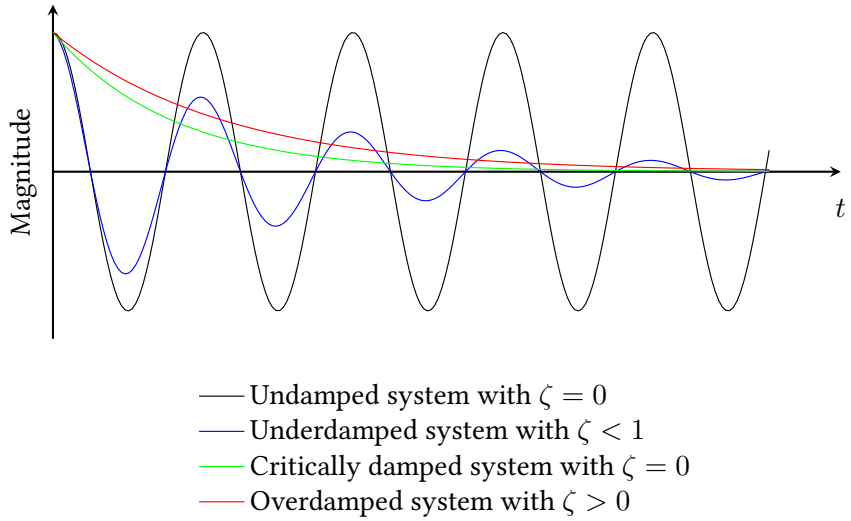

Figure 5.29: The oscillation of a damped system

This means in case of the vibraphone that the damping decays the oscillating motion within the time, whereby the slope of the envelope of the time domain curve describes the damping. In order to express the damping value, the envelope of the time domain curve can be analysed by means of the so-called Hilbert Transformation.

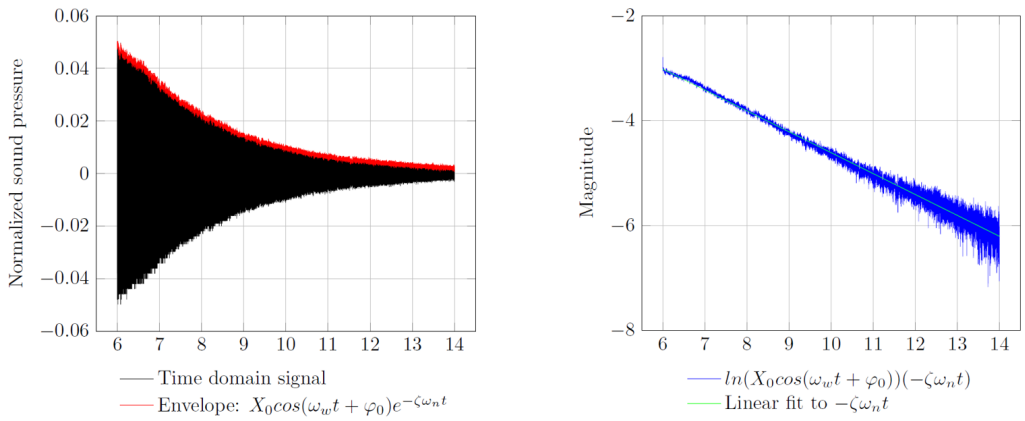

Figure 5.30: The damping of the vibraphone

The Hilbert Transformation is often applied to show a signal differently in one domain (mostly time domain), in comparison to the Fourier Transformation, which is mainly used to transform a signal from one domain to another domain. For further information about

the Hilbert Transformation it is referred to Guicking (2016). Within this work, the Hilbert Transformation is used to calculate the envelope of the time domain function: the black curve in figure 5.30 shows a cutout of the decaying pressure signal of the vibraphone in the time domain. The red curve is the signal which has been processed with the Hilbert Transformation, the so-called envelope of the time domain function. It can be seen, that the envelope $\varrho(t)$ consists of oscillating components and a decay function. This behaviour may be expressed by:

$$\varrho(t) = X_0 cos(\omega_w t + \varphi_0) e^{-\zeta\omega_n t}, \tag{5.20}$$

where the $e^{-\zeta\omega_n t}$ describes the decay of the oscillations with the slope of ζ (damping ratio). In order to calculate this slope, on the right hand side figure 5.30 shows the natural logarithm applied on the equation 5.20, which leads to the following expression:

$$ln(\varrho(t)) = ln(X_0 cos(\omega_w t + \varphi_0))(-\zeta\omega_n t). \tag{5.21}$$

In the next step, the oscillating motion $cos(\omega_w t + \varphi_0)$ may be neglected by applying a linear fit on equation 5.21: the slope of the fitted curve describes the damping ratio ζ. In this example a damping ratio of ζ = 0,0001441 of the vibraphone bar is determined, which means that the vibraphone has a small damping. (Norton & Karczub 2003)

In the next chapters the experiment is replicated in simulations with different methods and made audible by auralization. In the last chapter the simulation and experimental results are compared.

5.4.2 Simulation and Auralization

In this chapter the auralization method developed within this work (see figure 5.1) is applied on the vibraphone bar to mimic the experiment depicted in the previous chapter. On the left hand side, figure 5.31 shows the simulation model of the vibraphone bar. Basically, it consist of a vibraphone bar, a force and four constraints (see figure 5.32). The force is applied according to the experiment.

Furthermore, this simulation model is depicted without resonator because the auralization method does not take reflecting waves into account. Therefore, the function of the resonator can not be used within the simulation model. However, the resonator only amplifies the sound pressure level and does not change its time dependent variation of the sound pressure characteristics. As mentioned previously, the auralization method is not developed to calculate the exact amplitudes but rather to determine the time dependent variation of the sound pressure signal. In other words, the negligence of the resonator is a necessary and convenient step

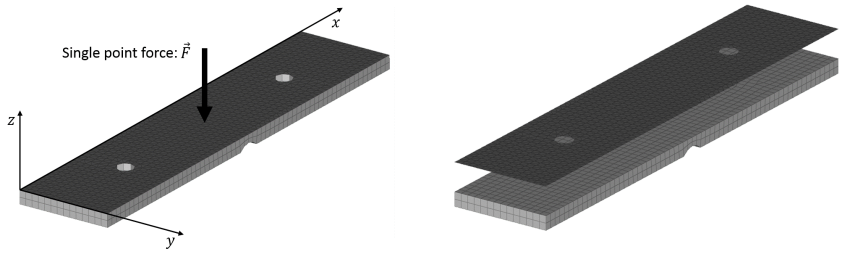

Figure 5.31: Simulation model of vibraphone bar

for the transient simulation in order to additionally decrease the computation time without changing any relevant characteristics for the method. In the first step of the auralization method the part gets discretized. Figure 5.31 shows the exploded view of the structure- and the surface mesh of the vibraphone bar model with the following characteristics:

Table 5.6: Mesh properties of vibraphone bar model

	Structure	Surface
Nodes	2907	969
Elements	1772	1768

Furthermore, figure 5.32 shows the bottom view of the bar which is fixed in z-direction in all four constraints (black crosses) because the bar of the real vibraphone lays on four soft rubber elements, which enormously increases the damping of these points compared to other points.

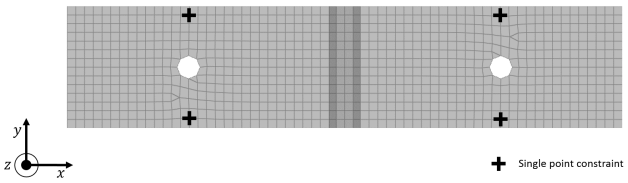

Figure 5.32: Bottom view of simulation model of vibraphone bar

Therefore, as simplification, the small vertical motion of the constraints of the real bar is assumed to be 0 within this simulation model due to reducing the computational effort. In the second step, a modal analysis is applied on the discretized bar to determine the eigenmodes. Figure 5.33 depicts the first five eigenmodes of the vibraphone bar and its original position (dashed). It can be seen, that the mode shapes do not show any motion in the area close to the

constraints due to the discussed restriction of the perpendicular motion of the bar. Furthermore, on the left hand side of figure 5.33, the first eigenmode of the vibraphone bar is depicted: this describes the motion of the bar at the fundamental frequency of 880 Hz and is therefore the dominant shape for the sound generation.

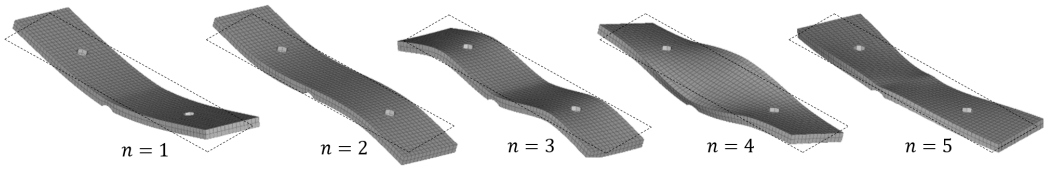

Figure 5.33: Eigenmodes of vibraphone bar

However, according to the principle of superposition more modes need to be included to reproduce the real body motion in the model (see figure 5.2). In this context, figure 5.34 shows the spectrum of the vertical displacement in the middle point (force exciting point) of the vibraphone bar. The normalized vertical displacement is shown on the y-axis because the absolute values of the displacement regarding frequencies are not relevant in this work. Furthermore, both axis are depicted in a logarithmic scale. For illustration purposes two curves are depicted: the dashed curve shows the frequency characteristics of 100 included modes and the continuous curve of 4 included modes. First, the amplitudes of both curves at 880 Hz are consistent with the theory of vibraphones because, as mentioned, vibraphones are designed to generate a tone of the fundamental frequency only (in this case 880 Hz).

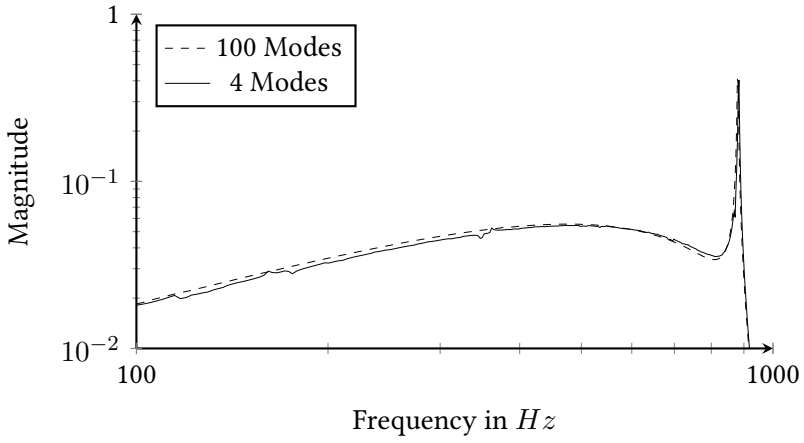

Figure 5.34: Influence of number of included modes on the body motion

Second, it can be seen, that the curve including more modes is smoother and without any fluctuations compared to the curve with less modes. I.e. the curve with 4 included modes reveals additional frequency components, which can results into a whirring noise in the sound signal. Basically, these characteristics confirm the theory that every motion consists of a summation of proportions of many modes and this means in case of a less amount of modes, that the motion can not precisely be calculated because the influence of the upper modes is missing. The inclusion of more modes will enhance accuracy. The generated sounds with different numbers of included modes are located in the attachment 'Vibraphone-4Modes.m4a' and 'Vibraphone-100Modes.m4a'.

Within this work the deformable rigid body simulation of the vibraphone is performed with 100 included modes because the generated sound is comprehensible with a very pure fundamental frequency of the bar. In addition, these amount of modes leads to an acceptable calculation time of 85 min.

Furthermore, the damping in the simulation model is defined according to the measured damping ratio of ζ = 0,000144 in the experiment (see chapter 5.4.1). The calculated damping ratio is considered as modal damping for all modes in the simulation model. In the next steps, the node output file of the vibraphone simulation is used in the auralization procedure. In this context, the auralization of the vibraphone signal does not differ from the ones in previous chapters and is therefore not described in detail here. Nevertheless, a few comments to the auralization of the vibraphone bar will be presented in the following sentences. A DC-Blocking filter is not needed in this model because no constant motion occurs. As illustrated in the previous examples, in the last steps, the sound pressure is determined at a given field point, buffered and finally converted into an audible result. The generated sound file is located in the attachment "Vibraphone.m4a".

In figure 5.35 the results of the auralization procedure are presented and on the left hand side the time domain result is depicted. The y-axis is shown as normalized pressure from -1 to 1 in a time interval from 0 to 5.0 s. It can be seen, that the time domain signal decreases very purely due to the damping.

However, in order to get more information of the generated sound, the time domain signal is transformed into frequency domain with a pure Fast-Fourier-Transformation as illustrated on the right hand side of figure 5.35. According to the validation, the frequency range is depicted from 100 Hz to 1000 Hz. Furthermore, a pure FFT is a transformation into the frequency domain without an applied window function in order to avoid interfering influences and to understand the real frequency characteristics. Furthermore, a FFT without a window leads to tiny mistakes when the time domain signal, like in this case, is not 0 at the start and end point

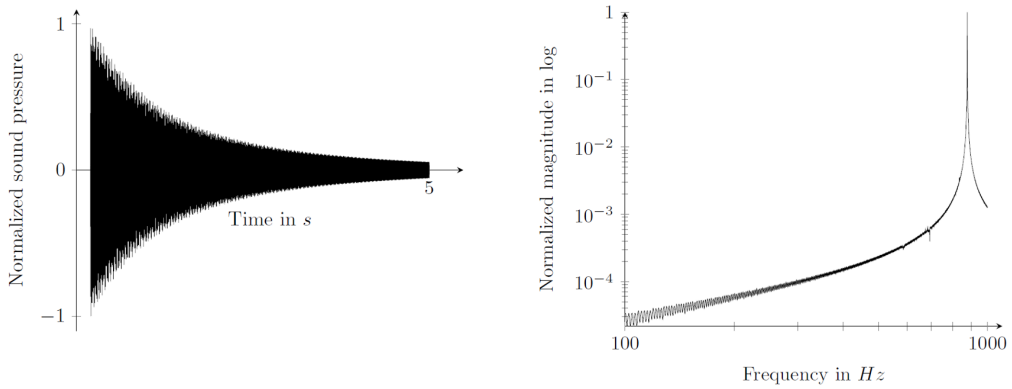

Figure 5.35: The time domain signal ouput of the auralization of the vibraphone bar motion in the time domain (left) and in the frequency domain (right)

of the transformation. These mistakes lead to the wave characteristics of the frequency curve, which can be seen especially in the front frequency area. Nevertheless, in order to compare the simulation to the experiment, it is of key importance to create curves with the same procedure and always as pure as possible. Therefore, all spectra for comparison are transformed without any applied window function. Besides that, the curve is very smooth with a clear amplitude at the fundamental frequency (880 Hz) of the vibraphone bar. Furthermore, in the frequency range from 590 Hz to 850 Hz some differing small peaks can be noticed. These peaks are a result of a large time step because the simulation is performed with an explicit calculation, which means that the time steps is not constant over time. For instance, a chosen time step of an explicit simulation of 1,00 s can be performed by the software as 0,99 s or 1,01 s. In general, choosing an explicit simulation is a good choice regarding calculating performance but its created data is burdensome to process due to the diverting time steps: the signal processing of the auralization method requires and expects a uniform time step. That means, the script assumes, that the previously chosen time step is true and does not take its real tiny differences into account. Therefore, within the auralization procedure, these time step differences are neglected, which lead to small mistakes in terms of these peaks. In order to decrease these mistakes a smaller time step can be used or the output sampling rate can be increased. In the example of the vibraphone bar, the output sampling rate is increased to 40000 Hz from $f_s \geq 2000$ Hz[9], in order to decrease the time step mistake as much as possible. In conclusion,

[9] According to chapter 4 an output sampling rate of $f_s \geq 2000$ Hz should be sufficient to cover all vibraphone frequencies up to 1000 Hz.

although these small peaks are not audible in this example, it can be in other cases: in next examples, it is of key importance to avoid the occurrence of additional frequency components by using a small time step or a high output sampling rate. Alternatively can be used implicit simulations.

This chapter shows how to simulate and auralize a musical instrument. The generated sound and the spectrum present comprehensible results. Especially the spectrum shows promising results, which are close to the theory of the vibraphone. In the next chapter the Boundary Element Method will be used to replicate the experiment. The validation of both simulation techniques and the experiment is presented in the last section of this chapter.

5.4.3 Boundary Element Simulation

The Boundary Element Simulation of the vibraphone bar is used within this work for additional validation purposes only. The objective is to evaluate, whether verifications of the transient acoustic simulation method can be done by using another simulation technique like the Boundary Element Method. For this reason, the BEM model is briefly explained: figure 5.36 depicts the simulation model. The components are: the vibraphone bar and the resonator. Furthermore, the field is meshed in order to calculate the sound propagation.

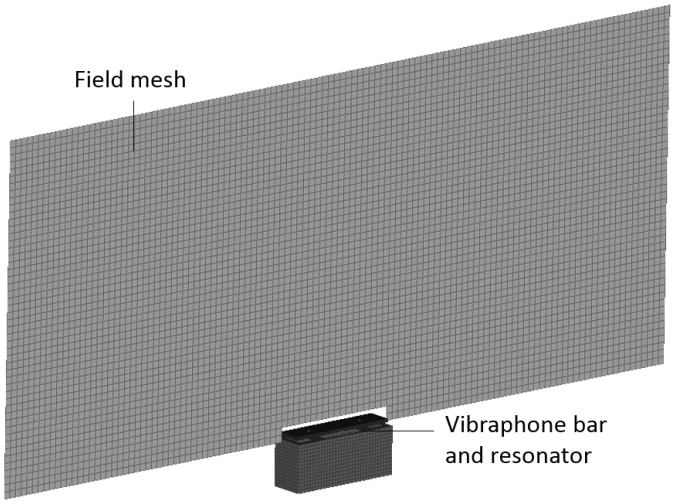

Figure 5.36: The vibraphone simulation model (Boundary Element Method)

The resonator is designed with a hard walled sound characteristics. I.e. the walls have a high impedance in order to reflect all incoming waves, which is close to reality and therefore convenient as simplification. In this BEM simulation, a so-called steady state simulation is used, which describes a simulation method in the frequency domain only with an equilibrium state (stationary process) and without any time dependency, whereby the mass and energy are always balanced. This method is chosen because it is independent from time: this is beneficial for the validation in the frequency domain because it is easier to understand the calculation results when no transformation within the solver is carried out. Therefore, at first the force and the damping from the experiment have to be transformed manually into the frequency domain by using FFT in order to include these values in the steady state simulation.

Figure 5.37 presents the sound pressure level in dB of the vibraphone bar at 880 Hz. Moreover, it represents the radiation characteristics of the bar: at the bottom of the sound field, the sound pressure level depicts amplitudes above the openings of the resonator and minimums above the constraints because of almost no motion occurrence in this area. However, more relevant is the wider radiation characteristic, which is according to the dipole characteristics (see figure 5.6) assumed to be circular within the auralization procedure: it turns out to be a very reasonable assumption for the vibraphone bar. However, in case of other bodies, other radiation characteristics can occur but in this context, BEM simulations can support to calculate the sound radiation characteristics in order to use this information in the auralization procedure of the transient simulation.

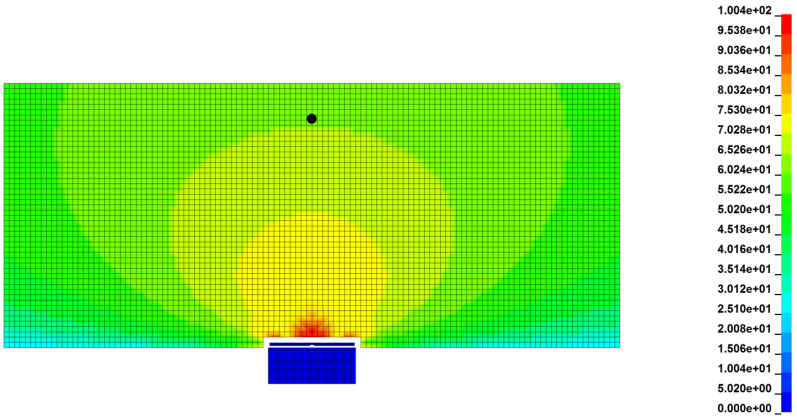

Figure 5.37: The sound propagation of the vibraphone bar at $880\ Hz$

Furthermore, the simulation is performed in a frequency range from 800 Hz to 1000 Hz to depict the area around the fundamental frequency and reduce calculation time[10]. Figure 5.38 shows the spectrum of the field point located 30 cm above the bar[11]. It depicts a smooth curve with a clear amplitude at the fundamental frequency (880 Hz). This curve is used for the validation.

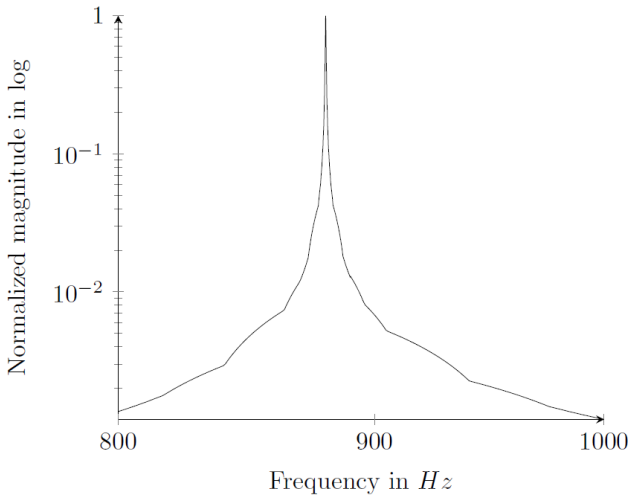

Figure 5.38: The spectrum of the field point (30 cm above the bar)

In the next chapter the experiment and simulation results are compared.

5.4.4 Validation

In this chapter, the frequency characteristics of the auralized transient simulation, the BEM simulation and the experiment are compared in the area around the fundamental frequency. As review, the y-axis is depicted as the normalized sound pressure because the auralization method determines the sound characteristics with an approximation of the amplitude only. The spectra of the experiment and the auralization method are transformed by FFT[12] from the decaying time domain signal after the excitation, in the time range from 2 s to 5 s in order to avoid influences of the different force excitations: in the simulation model, the excitation happens by one force (single point force) only, whereby in the experiment a planar contact occurs due to the geometry of the tip of the impact hammer. This can lead to other frequency

[10] BEM simulations calculate each frequency individually, which leads to long calculation times for a large frequency range.
[11] The location is depicted in figure 5.37 as black dot.
[12] As mentioned, all FFT are done without an application of a window function in order to avoid window influences.

components in the excitation time, but after the excitation, the vibraphone bar swings in its fundamental frequency and eliminates other frequency components. Therefore it is convenient to use the decaying part of the sound to enable a better evaluation of the applied method.

Now to the comparison of the curves: first, figure 5.39 depicts the frequency domain curves of the experiment and the generated sound from the transient simulation. It can be noticed that both curves are close to each other in all areas. Especially the area of the fundamental frequency (880 Hz) shows a close coincidence. The small difference of both curves in the frequency range from 100 Hz to approximately 450 Hz is negligible because the magnitudes are far below human hearing range. Furthermore, the hearing comparison of both sound files indicate no real difference for non-experts (see attachment: 'Vibraphone-Auralization.m4a' and 'Vibraphone-Experiment.m4a').

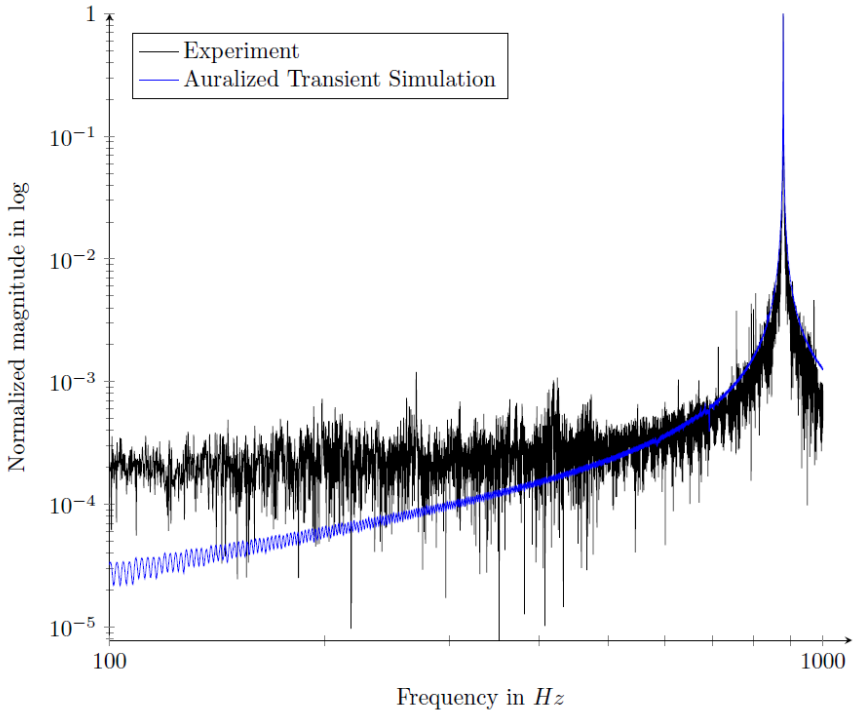

Figure 5.39: The frequency domain representation of the experiment and the auralized sound

Second, figure 5.40 presents both simulation results compared to the experiment in a range from 800 Hz to 1000 Hz in order to show closer the area of the fundamental frequency and

to depict the BEM result[13]. It can be seen that all three curves are close to each other with a clear fundamental frequency at 880 Hz. Furthermore, it is worth to mention, that both simulation curves are very close in all areas. This offers promising verifications possibility of the auralization technique by using BEM.

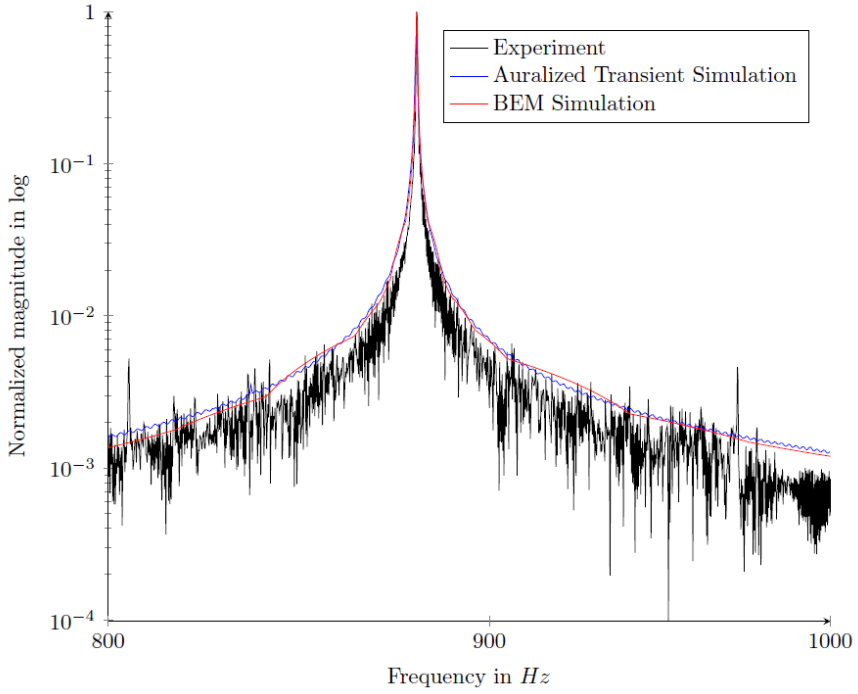

Figure 5.40: The frequency domain representation of the experiment, the auralized sound and the BEM simulation

The frequency curve of the auralized sound is very close to the experimentally determined quantities. It can be concluded that the applied auralization method is a suitable technique to generate a synthesized sounds of a vibraphone bar. Furthermore, it can be assumed that similar problems can be solved in the same accurate manner.

[13]The BEM simulation is performed in a range from 800 Hz to 1000 Hz only.

6 Conclusion

Based on known approaches from literature, within this work an approach is developed which is able to transfer numerical simulation results from commercial FE simulations into audible results (auralization). This approach finally generates audio results at given field points. For better performance simplifications like e.g. the modal methods and Huygens' Principle are taken into account.

In order to evaluate the developed approach, this work presents several examples with its application: the first example of the cantilever was used to evaluate the application of the method in a first attempt and to develop scripts. This example presented promising results especially regarding the quality of the generated audio file and its calculation time. However, a swinging metal can be assumed from the audio file but it was not possible to evaluate this in detail because no data from experiments was available. Therefore, in a next step an example with a known and easy to replicate sound was used: a ball dropping on a surface. This example showed comprehensible audible results. Especially the sound of the rolling ball on the table was very promising. After these two examples, it was of key importance to be able to quantify how close the results are to reality. In this context, the vibraphone was selected for the validation. Therefore, the carried out experiment in the acoustic chamber was compared with the generated sound by the developed method and for further verifications with the Boundary Element simulation. All three results were very close to each other, which indicates that the method is, especially for similar problems, close to reality.

In conclusion of this work, the method shows reasonable and promising results for the selected examples. Furthermore, the method has a good performance according to the preprocessing (creation of model) and the calculation time of the script through its simplifications. For further developments it is recommended to apply the method to more complex parts to identify its industrial usability. For some models, it can be useful to define a more complex approach with e.g. taking wave reflection and transmission into account. Furthermore, it is recommended to integrate other simulation techniques e.g. BEM for more complex radiation problems as support for better results.

Bibliography

Agilent Technologies (2012), *The Fundamentals of Signal Analysis*, USA.

Ammari, H. (2008), *An Introduction to Mathematics of Emerging Biomedical Imaging*, Springer-Verlag, Heidelberg.

Baader, R. (2002), *Fraktale Dimensionen, Informationsstrukturen und Mikrorhytmik der Einschwingungsvorgänge von Musikinstrumenten*, Dissertation, Universität Hamburg.

Blauert, J. (2005), *Communications Acoustics*, Springer-Verlag, Heidelberg.

Blitzenbauer, J., Franz, U., Schulz, A. & Mlekusch, B. (2005), *Coupling of Deformable Rigid Bodies with Finite Elements to Simulate FMVSS Head Impact*, 4. LS-DYNA Anwenderforum, Bamberg.

Blitzenbauer, J., Franz, U. & Schweizerhof, K. (2005), Deformable rigid bodies in ls-dyna with applications - merits and limits, 5th European Ls-Dyna Users Conference, Bamberg.

Born, M. & Wolf, E. (2003), *Principle of Optics*, 7 edn, Cambridge University Press, Cambridge.

Braess, H.-H. & Seiffert, U. (2013), *Vieweg Handbuch Kraftfahrzeugtechnik*, 7 edn, Springer Fachmedien Wiesbaden.

Chandler-Wilde, S. & Langdon, S. (2007), *Boundary Element Methods for Acoustics*, University of Reading, United Kingdom.

Chen, C. H. (2007), *Signal and Image Processing for Remote Sensing*, Taylor & Francis Group, CRC Press.

Chen-Yih, C. (1996), *Early Chinese Work in Natural Science*, Hong-Kong University Press, Hong-Kong.

Dassault Systèmes (2017), *Structural-Acoustic Simulation*, 10.01.2017.
URL: *http://www.3ds.com/products-services/simulia/products/abaqus/multiphysics/structural-acoustic-simulation/*

de Freitas, J. M. (2007), *The DC Blocking Filter*, QinetiQ Ltd, Dorchester.

DIN 55350-11:2008-05 (2008), *Begriffe zum Qualitätsmanagement - Teil 11: Ergänzung zu DIN EN ISO 9000:2005*, German Industry Norms.

Do, M., Baraniuk, R., Choi, H. & et al., B. F. (2012), *Fudamentals of Signal Processing*, Rice University, Texas.

Eichler, J. (2014), *Physik für das Ingenieurstudium*, 5 edn, Springer Fachmedien Wiesbaden.

Gaul, L., M.Kögl & Wagner, M. (2003), *Boundary Element Methods for Engineers and Scientists*, Springer-Verlag, Heidelberg.

Goodman, J. W. (2005), *Introduction to Fourier Optics*, 3 edn, Roberts & Company Publishers, Greenwood Village.

Guicking, D. (2016), *Schwingungen, Theorie und Anwendungen in der Mechanik, Akustik, Elektrik und Optik*, Springer Fachmedien, Wiesbaden.

Halliday, D., Resnick, R. & Walker, J. (2002), *Fundamentals of Physics, Part 3*, 6 edn, John Wiley & Sons, LTD, London.

Huang, Y. & Cui, Z. (2013), *Acoustics and NVH in LS-DYNA*, Infoday Acoustics and NVH-Analysis, DYNAmore 2013, 08.01.2017.
URL: *https://www.dynamore.de/en/downloads/infodays/dokumente/2014-Aku-ppt/3-dynamore-info-aku-huang-et-al.pdf*

Huygens, C. (1690), *Traité de la lumière (engl. Treatise on Light)*, translated by S.P. Thompson 1962, MacMillan and Co. Limited, London.

ISO EN 226:2003 (2014), *Acoustics - Normal equal-loudness-level contours*, International Organization for Standadization.

John H. Lienhard IV and John H. Lienhard V (2008), *A Heat Transfer Textbook*, 3 edn, Phlogiston Press, Cambridge.

Kalny, O. (2013), *Modal Analysis*, CSI Knowleedge Base, USA, 09.12.2016.
URL: *https://wiki.csiamerica.com/display/kb/Modal+analysis*

Kinsler, L., Frey, A., Coppens, A. & Sanders, J. V. (2000), *Fundamentals of Acoustics*, 4 edn, John Wiley and Sons, Inc., New York.

Lerch, R., Sessler, G. M. & Wolf, D. (2009), *Technische Akustik*, Springer-Verlag, Heidelberg.

Liljencrants, J. (2006), *End Correction at a Flue Pipe Mouth*, 07.01.2017.
URL: *http://www.fonema.se/mouthcorr/mouthcorr.htm*

Lone Star Percussions (2016), *Bergerault 3.0 Octave Performance Silver Aluminum Vibraphone*, USA, 28.12.2016.
URL: *http://www.lonestarpercussion.com/Keyboards/Vibraphones/Dynasty-3-0-Octave-Performance-Silver-Aluminum-Vibe-KVPS30G.html*

Mach, E. (1919), *The Science of Mechanics*, translated by T. J. McCormack, The Open Court Publishing Co., London.

Maker, B. N. & Benson, D. J. (2003), *Modal Methods for Transient Dynamik Analysis in LS-Dyna*, International LS-DYNA User Conference, CA, USA.

Miller, D. A. B. (2010), *Huygen's Wave Propagation Principle Corrected*, Vol. 16, ATT Bell Laboratories, Crawfords Corner Road, Holmdel, New Jersey.

Norton, M. P. & Karczub, D. G. (2003), *Fundamentals of Noise and Vibration Analysis for Engineers*, 2 edn, Cambridge University Press, New York.

O'Brien, J. F., Cook, P. R. & Essl, G. (2001), *Synthesizing Sounds from Physically Based Motion*, SIGGRAPH, Los Angeles.

Oppenheim, A. V., Schafer, R. W. & Buck, J. R. (1989), *Discrete-Time Signal Processing*, 1 edn, Prentice-Hall, Inc., New Jersey.

Oppenheim, A. V., Schafer, R. W. & Buck, J. R. (2008), *Auralization, Fundamentals of Acoustics, Modelling, Simulation, Algorithms and Acoustic Virtual Reality*, 1 edn, Springer-Verlag, Heidelberg.

Rossing, T. D. (2014), *Handbook of Acoustics*, Springer-Verlag, Heidelberg.

Russel, D. A. (2012), *Acoustics and Vibration Animations*, Graduate Program in Acoustics, The Pennsylvania State University, 17.05.2012.
URL: *http://www.acs.psu.edu/drussell/Demos/StandingWaves/StandingWaves.html*

Schönwald, N. (2010), Effiziente Simulation der Schallausbreitung in anwendungsnahen Triebwerkskonfigurationen, PhD thesis, Technical University Berlin.

Shin, K. & Hammond, J. K. (2007), *Fundamentals of Signal Processing*, John Wiley & Sons, LTD, London.

Siemens AG (2017), *LMS Virtual.Lab Acoustics für die Akustiksimulation*, 08.01.2017.
URL: *https://www.plm.automation.siemens.com/de_de/products/lms/virtual-lab/acoustics/index.shtml*

Tan, L. & Jiang, J. (2008), *Fundamentals of Analog and Digital Signal Processing*, 2 edn, AuthorHouse, Bloomington.

The Art of Hearing (2014), *How Human Ear Works*, 16.01.2017.
URL: *http://www.artofhearing.com.au/human-ear.html*

UdK Berlin (1998), *Pegelabnahme von Schalldruck und Schallintensität mit der Entfernung*, 08.01.2017.
URL: *http://www.sengpielaudio.com/PegelabnahmeVonSchalldruckUndIntensitaet.pdf*

Veselov, A. P. (2002), *Huygens' principle*.

Vorländer, M. (2008), *Auralization, Fundamentals of Acoustics, Modelling, Simulation, Algorithms and Acoustic Virtual Reality*, Springer-Verlag, Heidelberg.

Wendt, V. (2016), *Lecture Material of Acoustics*, Hamburg University of Applied Science.

Wiechmann, K. & Hiller, J. (2011), *Evaluation and Visualization of Equivalent Radiated Power in μETA*, 4th ANSA & μETA International Conference.

Will, P. (2017), *Lecture Material: DruckgradientenempfÃ¤nger: Akustische Übertragungsfunktion*, Mittweida Universtiy of Applied Science, 08.01.2017.
URL: *http://www.staff.hs-mittweida.de/pwill/diagram.html*

Wrobel, L. C. (2002), *The Boundary Element Method*, 1 edn, John Wiley & Sons, LTD, London.

Zeller, P. (2012), *Handbuch Fahrzeugakustik*, 2 edn, Springer Fachmedien Wiesbaden.

Hochschule für Angewandte Wissenschaften Hamburg
Hamburg University of Applied Sciences

Erklärung zur selbstständigen Bearbeitung einer Abschlussarbeit

Gemäß der Allgemeinen Prüfungs- und Studienordnung ist zusammen mit der Abschlussarbeit eine schriftliche Erklärung abzugeben, in der der Studierende bestätigt, dass die Abschlussarbeit „– bei einer Gruppenarbeit die entsprechend gekennzeichneten Teile der Arbeit [(§ 18 Abs. 1 APSO-TI-BM bzw. § 21 Abs. 1 APSO-INGI)] – ohne fremde Hilfe selbständig verfasst und nur die angegebenen Quellen und Hilfsmittel benutzt wurden. Wörtlich oder dem Sinn nach aus anderen Werken entnommene Stellen sind unter Angabe der Quellen kenntlich zu machen."

Quelle: § 16 Abs. 5 APSO-TI-BM bzw. § 15 Abs. 6 APSO-INGI

Dieses Blatt, mit der folgenden Erklärung, ist nach Fertigstellung der Abschlussarbeit durch den Studierenden auszufüllen und jeweils mit Originalunterschrift als letztes Blatt in das Prüfungsexemplar der Abschlussarbeit einzubinden.
Eine unrichtig abgegebene Erklärung kann -auch nachträglich- zur Ungültigkeit des Studienabschlusses führen.

Erklärung zur selbstständigen Bearbeitung der Arbeit

Hiermit versichere ich,

Name: _____

Vorname: _____

dass ich die vorliegende – bzw. bei einer Gruppenarbeit die entsprechend gekennzeichneten Teile der Arbeit – mit dem Thema:

ohne fremde Hilfe selbständig verfasst und nur die angegebenen Quellen und Hilfsmittel benutzt habe. Wörtlich oder dem Sinn nach aus anderen Werken entnommene Stellen sind unter Angabe der Quellen kenntlich gemacht.

- die folgende Aussage ist bei Gruppenarbeiten auszufüllen und entfällt bei Einzelarbeiten -

Die Kennzeichnung der von mir erstellten und verantworteten Teile der ist erfolgt durch:

Ort	Datum	Unterschrift im Original